

R-06-17

Modelling of the state of stress

Preliminary site description Laxemar subarea – version 1.2

Eva Hakami, Ki-Bok Min
Itasca Geomekanik AB

December 2009

Svensk Kärnbränslehantering AB
Swedish Nuclear Fuel
and Waste Management Co
Box 250, SE-101 24 Stockholm
Phone +46 8 459 84 00



Modelling of the state of stress

Preliminary site description Laxemar subarea – version 1.2

Eva Hakami, Ki-Bok Min
Itasca Geomekanik AB

December 2009

This report concerns a study which was conducted for SKB. The conclusions and viewpoints presented in the report are those of the authors. SKB may draw modified conclusions, based on additional literature sources and/or expert opinions.

A pdf version of this document can be downloaded from www.skb.se.

Summary

Aiming to work out a plausible description of the prevailing in situ stresses at Laxemar, a candidate site for a future permanent repository, results from stress measurements carried out in four boreholes within the investigated area have been used, together with already existing data from the region. In situ stress measurements have been performed by both hydraulic fracturing and overcoring technique. The data show a general depth dependence for the stress magnitude, as expected, but a fairly large variation between boreholes. The general orientation of the major principal stress is northwest-southeast.

With the presumption that the major deformation zones, crossing all over through the subarea, have played the major role in producing the current distribution of in situ stresses, the distinct element program 3DEC was used to construct a numerical models in which the major deformation zones; already characterized through comprehensive geological surveys, were incorporated. A three-dimensional numerical analysis was conducted by initializing stresses in the model block, containing a simplified structure geological layout of the subarea. The stresses at the boundaries are kept constant at assumed stress levels in three different cases. The lower strength properties in the deformation zones cause some slip on the zones, depending on stress levels and orientation. Stress values at corresponding points in the model are compared to measured values in the boreholes. The final state of stress in the numerical model, for the case that is closest to measurement values, is considered to show a plausible state of stress at the site.

While the deformation zones modelled are the expected cause for local variation of the stress field it was possible to distinguish two stress domains, I and II. Stress domain II, with expected lower stresses, is the rock mass above the wedges formed by deformation zones between ZSMEW002 and ZSMEW007 in Laxemar subarea, and below Ävrö and Hälö islands in Simpevarp subarea.

Sammanfattning

Med målet att ta fram god beskrivning av de bergsspänningsförhållanden som råder vid Laxemars kandidat område för ett framtida slutförvar för kärnbränsleavfall har resultat använts från bergspänningsmätningar i fyra borrhål. Bergspänningsmätningar har utförts med både hydraulisk spräckningsmetod och överborrningsmetod. Under antagandet att de större deformationszonerna, som korsar genom hela undersökningsområdet, spelar en betydande roll för hur spänningsförhållandena ser ut så konstruerades en numerisk modell i 3DEC (en diskret elementmodell) där deformationszonerna inkluderades. Deformationszonernas karakteristik är beskriven genom det omfattande arbetet med geologiska undersökningar. Det huvudsakliga kriteriet för att inkludera en deformationszon i modellen för spänningsfördelning var en minsta uppskattad zonbredd om 50 meter.

Den tredimensionella numeriska analysen gjordes genom att låta modellblocket, som innehöll sprickplanen som motsvarar förenklade deformationszoner, komprimeras inåt från två motstående sidor medan de andra sidorna ej tilläts expandera utåt. En ökning och omfördelning av spänningar fås i modellen och komprimering fortgår tills beräknade spänningsvärden i lägen motsvarande mätpunkter ligger i nivå med uppmätta spänningsvärden. Den spänningsvariation som fås i den numeriska modellen antas så representera den verkliga spänningsfördelningen i studerat område.

Eftersom de modellerade deformationszonerna är det som förväntas varatt upphov till lokal variation i bergspänningsfältet var det möjligt att dela in området i två spänningsdomäner, I och II. Spänningsdomän II som har en lägre förväntad spänning, är de kilformade bergvolymerna som bildas mellan zonerna ZSMEW002 och ZSMEW007 i delområdet Laxemar och under Ävrö och Hålö (zonerna ZSMNE012A och ZSMN024A) i Simpevarps delområde.

Contents

1	Introduction	7
1.1	Background	7
2	Stress Measurement Data	9
2.1	Stress data used	9
2.2	Principal stress magnitudes	9
2.2.1	Maximum principal stress	9
2.2.2	Minimum principal stress	11
2.2.3	Intermediate principal stress	12
2.3	Results from hydraulic stress measurements	12
2.3.1	Minor horizontal stress magnitudes from hydraulic tests	12
2.3.2	Major horizontal stress magnitudes from hydraulic tests	15
2.3.3	Vertical stress magnitudes from hydraulic tests	15
2.4	Orientation of principal stresses	15
2.5	Stress data on a regional scale	16
2.6	Conclusions based on stress measurement data	16
3	Numerical modelling of the stress variation	17
3.1	Objective and scope of the study	17
3.2	Deformation zones in the numerical model	17
3.3	Numerical model size and boundary conditions	21
3.4	Mechanical properties of the numerical model	22
3.5	Stress distribution in vertical and horizontal sections	24
3.6	Comparison between measured and modelled in situ stresses	30
3.6.1	Comparison in borehole KLX04	30
3.6.2	Comparison in borehole KAV04A	32
3.6.3	Comparison in Borehole KLX02	32
3.6.4	Comparison with the Äspö area	34
3.7	Effect of friction angle	35
3.8	Effect of change in zone ZSMNE012A termination	35
3.9	Conclusions from numerical modelling	39
4	Model for the state of stress at Laxemar	41
4.1	Stress domains	41
4.2	Model for principal stress magnitudes	43
4.3	Model for principal stress orientations	44
4.4	Uncertainty and variation in the stress model	44
	References	45

1 Introduction

1.1 Background

In situ rock stresses is one of the conditions that should be taken into account in the assessment of the suitability of a repository site. The in situ rock stress may also influence the design and construction of the repository. Therefore, as a part of SKB site investigation programme and the characterization efforts for the Laxemar site, this study is performed to establish a model for the focused area at Laxemar /SKB 2006/. The methodology used to perform the modelling of the state of stress follows the strategy outlined in /Hakami et al. 2002/. The modelling presented here is an update of the model presented in the site description for the Simpevarp subarea in /Hakami and Min 2005/, where the differences are due to changes in the geological model description and in the available measurement data.

The first step in the stress modelling is to compile and analyse the available measurement data and this step is presented in Chapter 2. The next step is that the geometry of the geological model and the deformation zone model are included in a three-dimensional numerical model simulating the stress variation. This numerical modelling study is described in Chapter 3. As the last step in the modelling the data and the numerical modelling are together forming the basis for the selection of the most relevant prediction for the state of stress at the Laxemar model volume, denoted the “stress model”. The model and its uncertainties are discussed in Chapter 4.

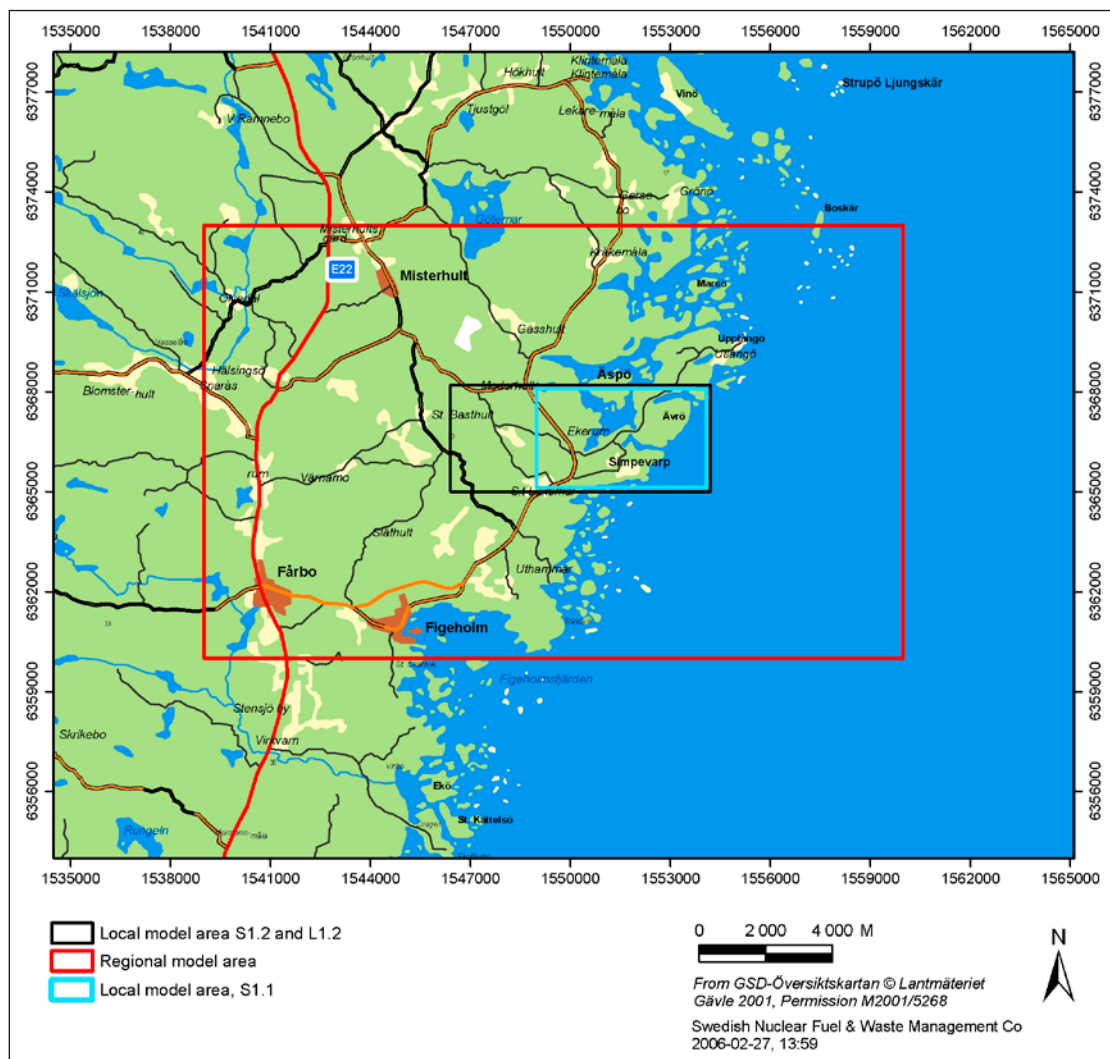


Figure I-1. Regional and local model areas used for Laxemar 1.2 /SKB 2006/.

2 Stress Measurement Data

2.1 Stress data used

Rock stresses have been measured in four new cored boreholes as part of the site investigation program at the Simpevarp and Laxemar subareas, namely in KSH01A, KSH02, KAV04A and KLX04. Note that data from borehole KLX04 were not included in the “data freeze” in connection to modelling Laxemar stage 1.2. However, during the course of this study data from KLX04 – to the extent that it was made available – were also used for this study. The location of these boreholes can be seen in Figure 2-1. Apart from these new data some older data from the time of the construction of the CLAB facility have been used. Further, measurement data from the Äspö Hard Rock Laboratory and data from a borehole (KOV01) in Oskarshamn (30 km south of Simpevarp) were also analysed, see Table 2-1.

2.2 Principal stress magnitudes

2.2.1 Maximum principal stress

Figure 2-2 shows the overcoring measurement results for the maximum principal stress. Each point in the diagram represents one single measurement and measurements in the same borehole are given the same symbol. A general increase in the stress magnitude with depth is observed, but the spread in the data from 400–500 m depth is large, with most data between 15 and 40 MPa, a single point around 10 MPa in KSH02 and two single points around 55 MPa at the Äspö laboratory (see map in Figure 2-1).

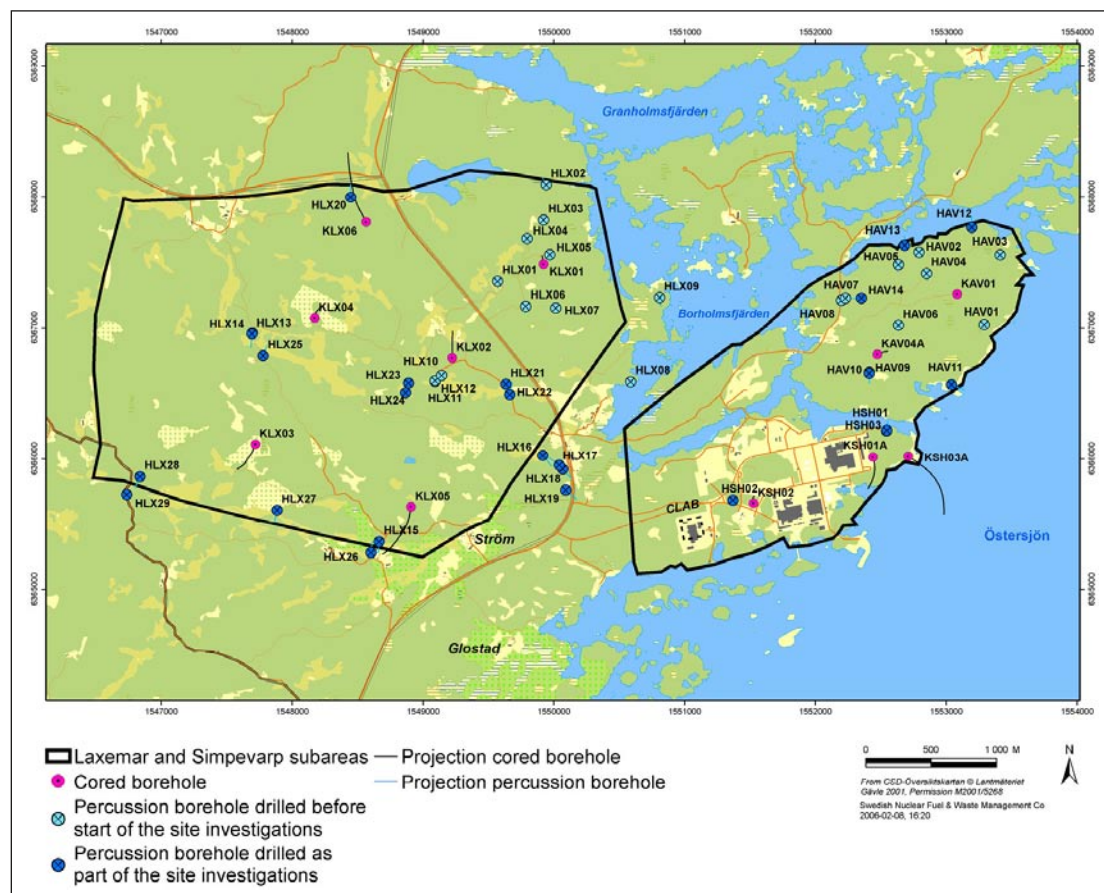


Figure 2-1. Overview map of core-drilled and percussion-drilled boreholes in the Laxemar and Simpevarp subareas. Stress measurements were made in boreholes KSH01A, KSH02, KAV04A, KLX04 and old data were available from Äspö Hard Rock Laboratory and CLAB.

Table 2-1. Available rock stress data for Simpevarp, version 1.2.

Data specification and borehole name	Meas. report SKB No.	Reference
Overcoring data from the site investigation program:		
KSH02	P-04-23	/Sjöberg 2004b/
KAV04A	P-04-84	/Sjöberg 2004a/
KLX04	P-05-69	/Sjöberg and Perman 2005/
Hydraulic fracturing data from the site investigation program:		
KSH01A	P-04-310	/Lindfors 2004/
Older overcoring data from the region:		
KF0093A01	R-02-26	/Janson and Stigsson 2002/
KA3376B01	IPR-03-16	/Sjöberg 2003/
KAS05	PR-25-89-17	/Bjarnason et al. 1989/
KOV01	IPR-02-18	/Klasson et al. 2002/
KK0045G01	IPR-01-67	/Klasson et al. 2001/
KA3579G	IPR-01-67	/Klasson et al. 2001/
Older hydraulic fracturing data from the region:		
KOV01	IPR-02-01	/Rummel et al. 2002/
KA2599G01	IPR-02-02	/Klee and Rummel 2002/
KF0093A01	IPR-02-02	/Klee and Rummel 2002/
KLX02	PR U-97-27	/Ljunggren and Klasson 1997/
KAS02, KAS03	PR-25-89-17	/Bjarnason et al. 1989/
P-wave velocity, transverse borehole core:		
KSH01A	P-03-106	/Chryssanthakis 2003/
KSH02	P-04-11	/Chryssanthakis 2004a/
KAV01	P-04-43	/Chryssanthakis 2004b/
KLX02	P-04-45	/Chryssanthakis 2004c/

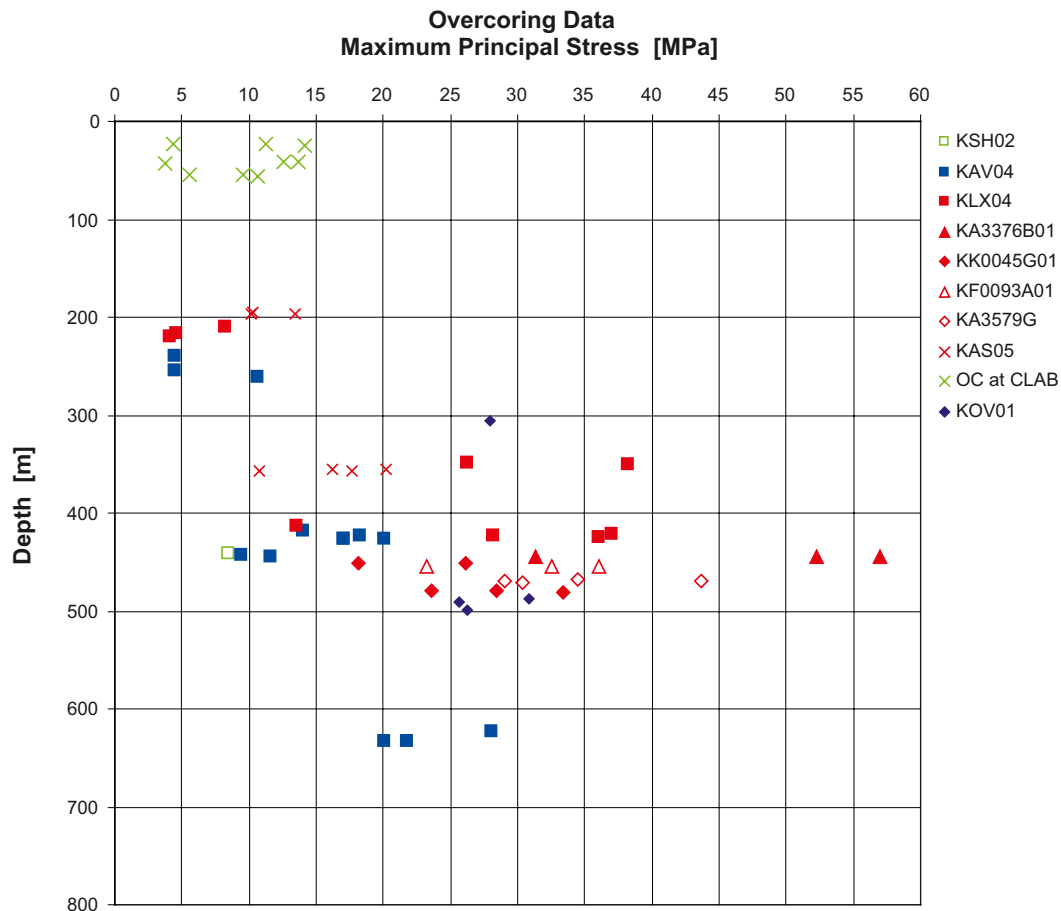


Figure 2-2. Results from the overcoring stress measurements from different boreholes in the area. The maximum principal stress magnitudes are shown.

However the measurements from the same measurement level in the same borehole generally give results within a 5–10 MPa wide span. Note further that only one borehole give data from below 500 m depth.

The data fairly close to the ground surface show maximum principal stress magnitudes clearly higher than the weight of overburden. Such stress regime is commonly seen in the whole Sweden, being a part of the Fennoscandian shield and is explained by the tectonic forces /Hakami et al. 2002/. The measurements at CLAB are scattered and these data have slightly less confidence since measurements are quite old and the overcoring techniques has developed further during recent years.

2.2.2 Minimum principal stress

The measurement results for the minimum principal stress, measured in the same points as for the maximum principal stress, are presented in Figure 2-3. The minimum principal stress values also vary fairly much between data points, but there is a clear trend for increasing magnitudes with depth, as expected. Again, it may be noted that the stress values obtained from points close to each other in the same boreholes have less spread compared to the overall spread.

Some of the measurement points indicate tensile stresses as the minimum principal stress, which is not very uncommon result from overcoring measurements. The minimum principal stress seems to be generally lower than the weight of overburden, which with an assumed density of about 2,700 kg/m³ is 10–13 MPa at 400–500 m depth. Such stress regime ($\sigma_1 > \sigma_v > \sigma_3$, assuming σ_1 and σ_3 being sub-horizontal) is called strike-slip and is not uncommon in Sweden.

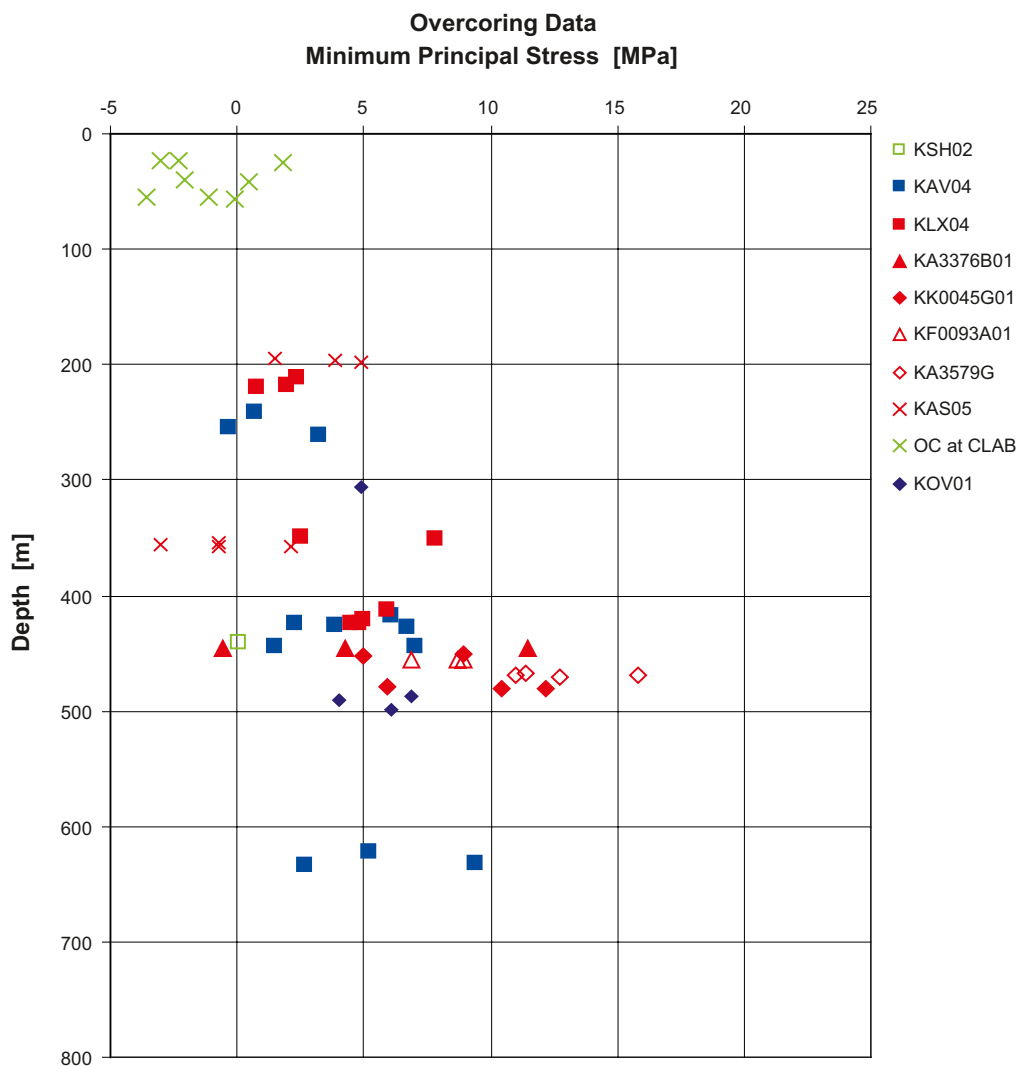


Figure 2-3. Results from the overcoring stress measurement. The minimum principal stress magnitudes are shown.

2.2.3 Intermediate principal stress

The measured intermediate principal stress, σ_2 , with the overcoring technique is presented in Figure 2-4. The intermediate stress also shows a general increase of stress magnitude with depth. The general picture is the same as for the maximum and minimum principal stresses. The intermediate magnitude appears to generally be closer to the minimum principal stress magnitude than to the maximum stress magnitude. The relations between principal stresses (or the stress anisotropy) may in addition be studied by looking at plots of the ratios (σ_1/σ_2 , σ_1/σ_3 and σ_2/σ_3) which are given in Figure 2-5.

2.3 Results from hydraulic stress measurements

2.3.1 Minor horizontal stress magnitudes from hydraulic tests

Within the site investigations for Laxemar stage 1.2 one attempt to do hydraulic tests has been performed, and this is in borehole KSH01A at Simpevarp peninsula. Hydraulic test data are further available from two boreholes drilled from the Äspö island ground surface (KAS02 and KAS03) and two shorter boreholes from inside the Äspö laboratory, KA2599G01 and KF0093A01. In Oskarshamn city hydraulic tests were performed in KOV01 at SKB's canister laboratory.

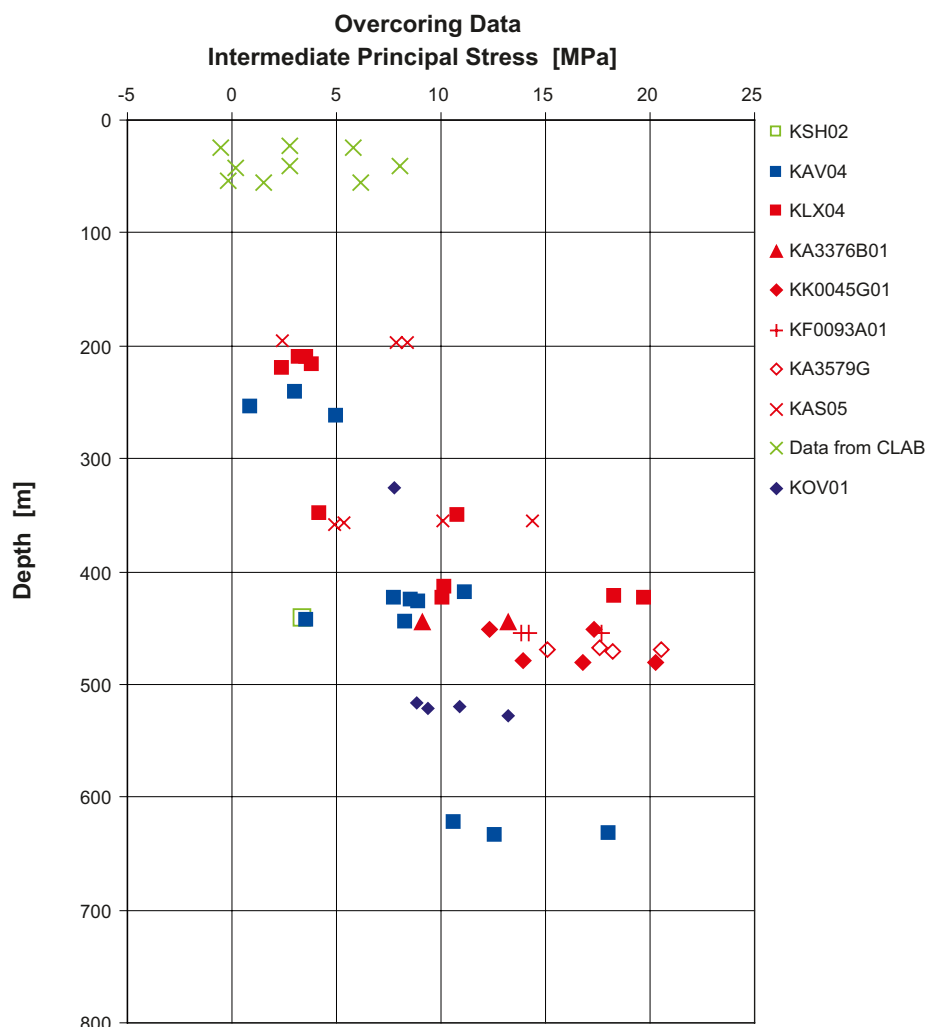


Figure 2-4. Results from overcoring stress measurements. The intermediate principal stress is shown.

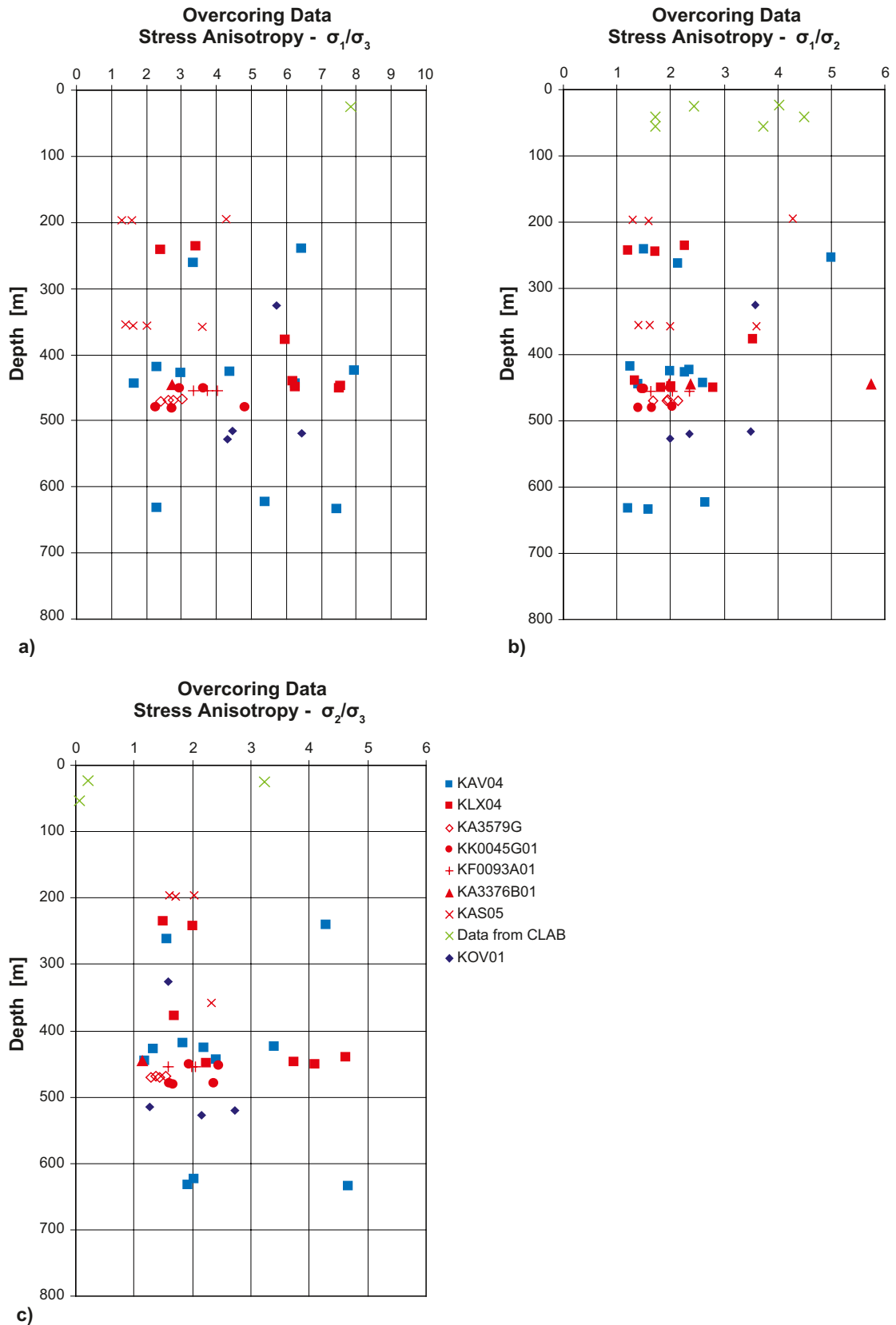


Figure 2-5. The ratio between the different principal stress magnitudes: a) σ_1/σ_3 , b) σ_1/σ_2 and c) σ_2/σ_3 . Note that some values fall outside the span of the x-axes of the diagrams.

The results from these tests in terms of the determined minimum principal stress magnitudes are shown for all boreholes together in Figure 2-6. From this diagram it may be concluded that the minimum stress magnitude shows, as expected, a general increase with depth. It may also be noted that there seems to be a fairly strong correlation between measurement points close to each other in the same borehole, i.e. the data scatter does not seem to be fully random.

In contrast to the overcoring data the hydraulic fracturing method gives data also from below 500 m depth. However, there are quite large differences in the results from the different boreholes at these depths. The hydraulic fracturing results indicate that the stress increase with depth is not a simple linear function in a particular borehole. The stress gradient variation is not similar in different boreholes, thus indicating that local factors (actual stress variation or possibly test procedure related) influence the measured stresses.

As a rough comparison between the different measurement method results, all the minimum principal stress values as determined with overcoring are compared to all the minor horizontal stress values determined through hydraulic fracturing in Figure 2-7. Since the measurements from different methods are not taken at the same points, or even in the same boreholes, the comparison is not fully proper to do, but with this in mind, it seems that there might be a systematic difference in that overcoring estimates lower minimum stresses than the hydraulic fracturing method. In particular, there is a clear difference in results from KOV01 and KF0093A01, where both overcoring and hydraulic measurements are made in the same hole (cf. Figure 2-3 and Figure 2-6). Such possible systematic measurement difference should be considered further in the description of uncertainty and confidence of the model of state of stress. One possible contributing factor to discrepancy is the difference in the orientation of measured stresses (minor principal vs. minor horizontal) and the orientation data is studied in next section.

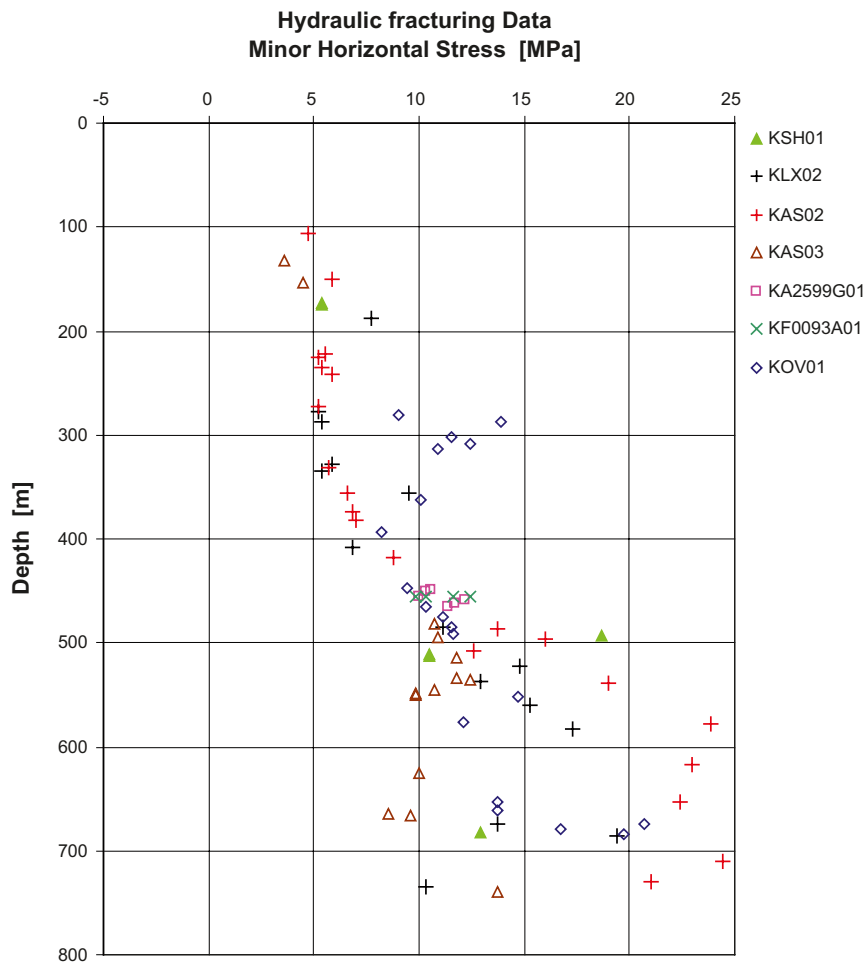


Figure 2-6. Minor horizontal stress determined with hydraulic fracturing tests in different boreholes in the Laxemar area with surroundings.

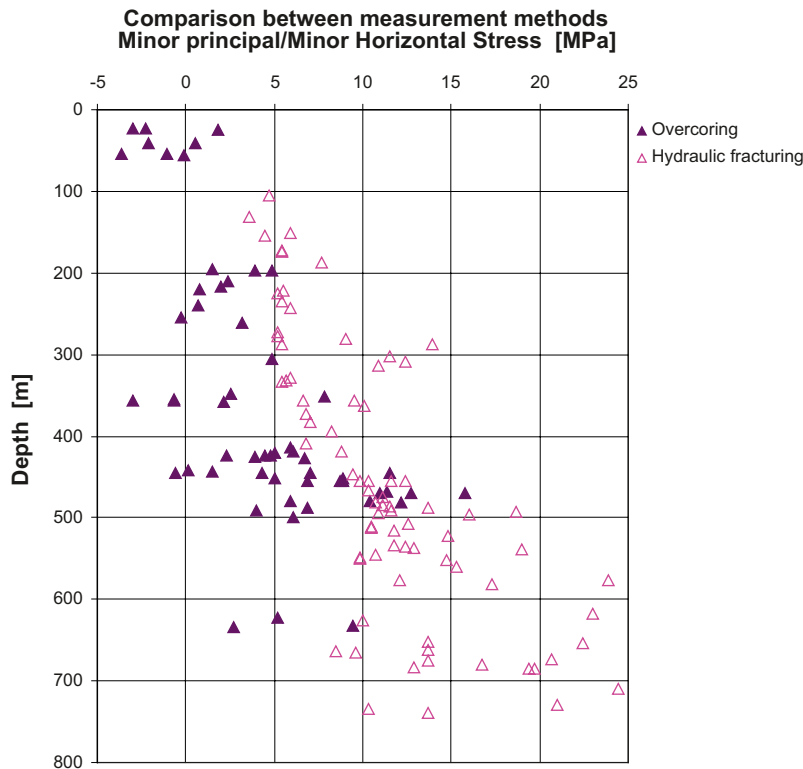


Figure 2-7. All available measurement data from the Laxemar area and surroundings for the minimum principal stress (overcoring) and minor horizontal stress (hydraulic fracturing), respectively. (Figure 2-3 and Figure 2-6 present these results separately).

2.3.2 Major horizontal stress magnitudes from hydraulic tests

The maximum horizontal stress magnitude is also often interpreted from hydraulic fracturing measurements, and such results are available in Sicada. However, following the strategy report for stress modelling /Hakami et al. 2002/, these data are not used for building the stress model, since there is a low confidence in the major horizontal stress parameter determined from hydraulic tests.

2.3.3 Vertical stress magnitudes from hydraulic tests

Using the hydraulic fracturing method the vertical stress may only be measured if the induced fracture plane is oriented horizontally, and since the objective of hydraulic fracturing measurements are most often to determine the horizontal stresses the tests are using vertical boreholes and aiming at vertical induced fracture planes. For this modelling work we have not used the hydraulic fracturing data to estimate the vertical stress.

2.4 Orientation of principal stresses

Figure 2-8 shows the orientation of the maximum principal stresses estimated from overcoring measurements together with the orientation for the major horizontal stress obtained from hydraulic fracturing measurements. The major principal stress is normally almost horizontally, and to get an overview it was therefore here chosen to present the data from both methods (principal stress in overcoring case and horizontal direction for hydraulic tests) together. The overall spread in the stress orientation data is large, but there is a clear concentration around NW-SE.

The scatter in stress magnitudes observed in Figure 2-2 and Figure 2-3 may be explained both as a result of the uncertainty in the measurement method itself, or as a result of a true spread in the stress magnitudes and orientations. It is probably that both factors do contribute to some extent to the spread. It is not possible, however, to show how much each of the two factors influence the data

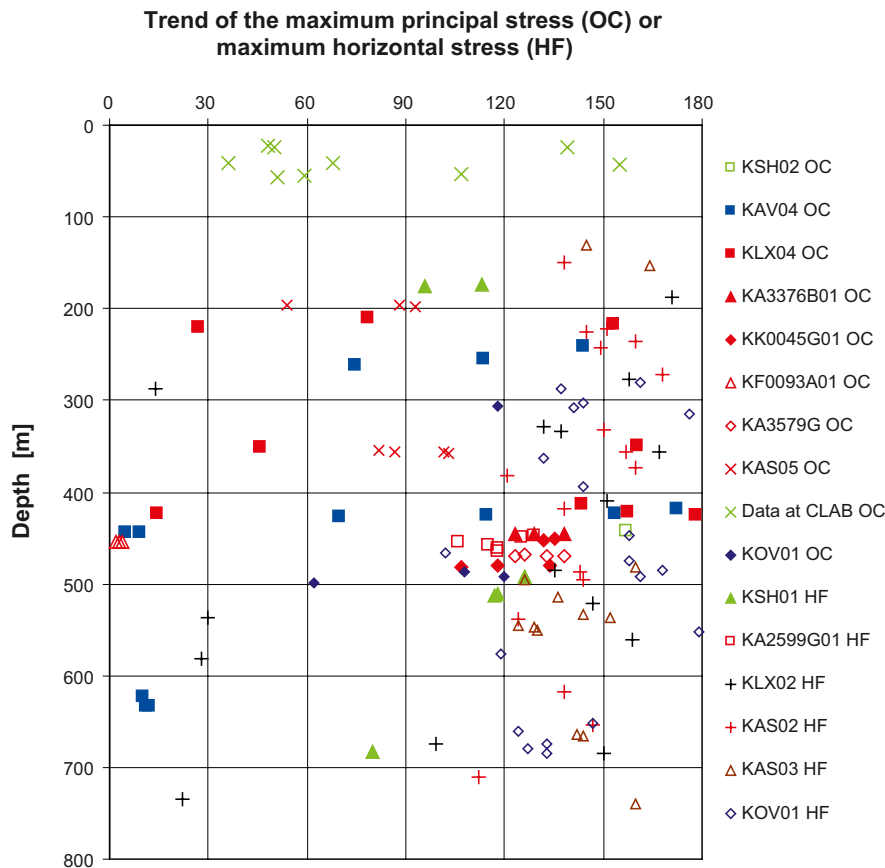


Figure 2-8. Orientation of maximum principal stress (overcoring) and major horizontal (hydraulic fracturing) measured in the Laxemar-Simpevarp area (the same data points as in Figure 2-3 and Figure 2-6).

in this case. In the modelling, it is assumed that the scatter in data represents a real stress variation and also that there is no systematic error in the data. The way the measurement data were used to establish the final descriptive model is described in Section 4.3.

2.5 Stress data on a regional scale

Considering available stress data on a larger scale, from the whole northern Europe, it may be concluded that there is a clear general trend to have the maximum compressive stress in the horizontal northwest-southeast direction. This is in agreement with the current understanding of the relative tectonic plate movements, which is the main cause for the compressive stress field. The stress field on a larger scale is brought up further in the strategy report for stress modeling /Hakami et al. 2002/.

2.6 Conclusions based on stress measurement data

From the compilation of the primary stress data and the discussion in the previous sections it may be concluded that the orientation of the major principal stress in the Laxemar local model area seems to coincide with the known orientation pattern in the northern Europe, having a preferred NW-SE trend. The stress magnitudes in the Laxemar local model area, as obtained from the measurement data, are within the range seen from other locations in Sweden, but the spread in data is large.

The variation in the stress magnitudes data within the area is large enough to motivate a division into different stress domains. A potential explanation to the variation in stress magnitudes will be sought in the structure geological conditions specific to the site. In the next chapter the attempt to numerically analyse the potential influence from the larger deformation zones on the stress distribution in the model area is presented.

3 Numerical modelling of the stress variation

3.1 Objective and scope of the study

The objective of the numerical model was to investigate the effect that the most important major deformation zones may have had on the current in situ stress field at the Laxemar local model volume. The objective have been to gain insight into the state of stress based on the current understanding of geological structures in the area, and this may be changed in the future since the geological modelling still continues. Furthermore, the modelling is using the results of the currently available stress measurement data which also may influence future modelling versions.

3.2 Deformation zones in the numerical model

Geological structures in the region around Laxemar model area (version 1.2) were characterized through various methods. These included surface mapping and geophysical surveys. The detailed description of the geological modelling work is published in the site description report /SKB 2006/. According to the generated deformation zone model, many deformation zones exist in the model volume as shown in Figure 3-1.

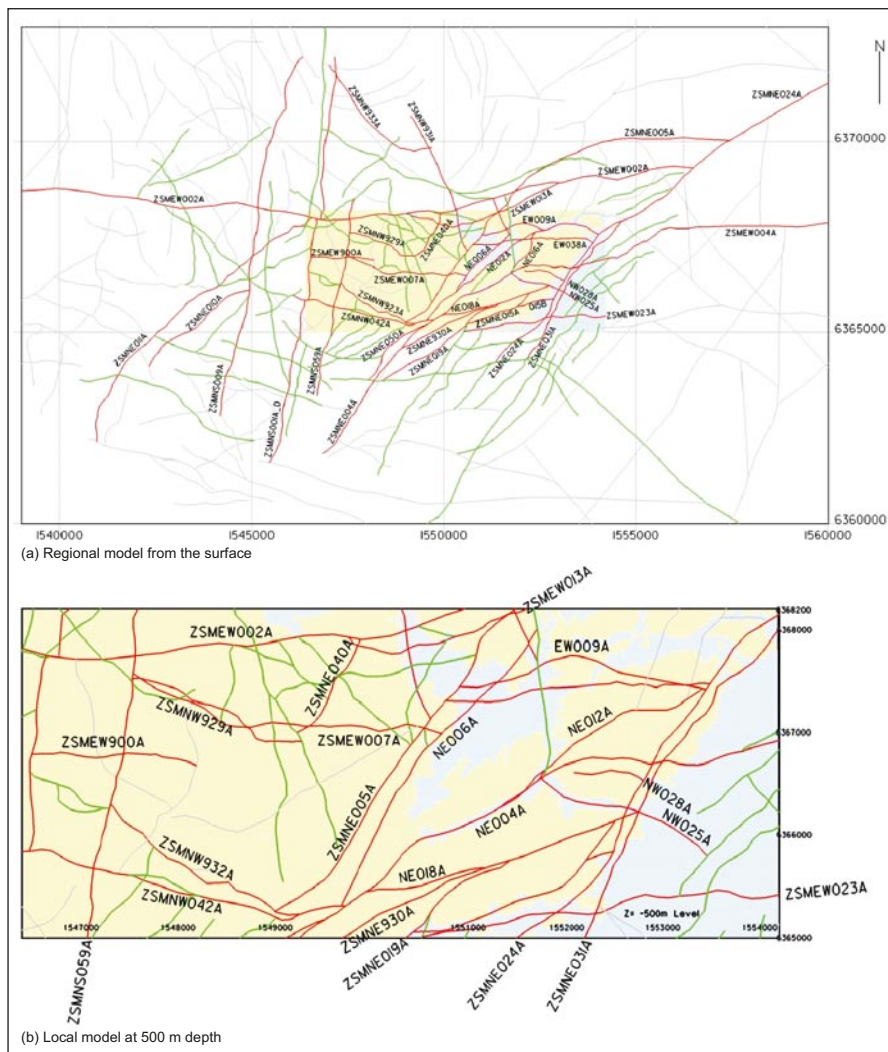


Figure 3-1. Deformation zones at Laxemar; model version 1.2. a) shows the zones in regional scale and b) shows the local model area with deformation zones in the horizontal plane at 500 m depth, which is the anticipated depth for the future repository /SKB 2006/. Red and green denotes different degree of certainty in the existence of zone.

Deformation zones were modelled at different resolution in the local and regional model volumes. Therefore the number of deformation zones is higher in the local model volume. The stress comparisons were however only carried out within the local model.

In the numerical model the large scale deformation zones from the geological model were simplified and modelled as planar discontinuities cutting through the model block. Figure 3-2 shows the deformation zones incorporated in the model. The details of deformation zones are listed in Table 3-2. The deformation zones that could have significantly influenced the stress regime were included in the model. The criterion for including a zone was 1) that it had an estimated width of 50 m and 2) that it was geometrically located such that it would influence the local volume. In certain cases, two deformation zones with smaller widths were merged and included in the modelling when they ran close to each other and had similar orientations.

Important borehole locations and reference sections made for the investigations are also shown in Figure 3-2. Sections AA' and BB' run parallel with the direction of the major principal stress; and pass through the centre of the Laxemar subarea and the location of borehole KAV04A, respectively. Section CC' passes through the centre of the local model and runs west-east. Sections DD' and EE' run close to each other in north-south direction, passing through the locations of borehole KLX06 and KLX04, respectively. The corner coordinates of the regional model and the local model are listed in Table 3-1.

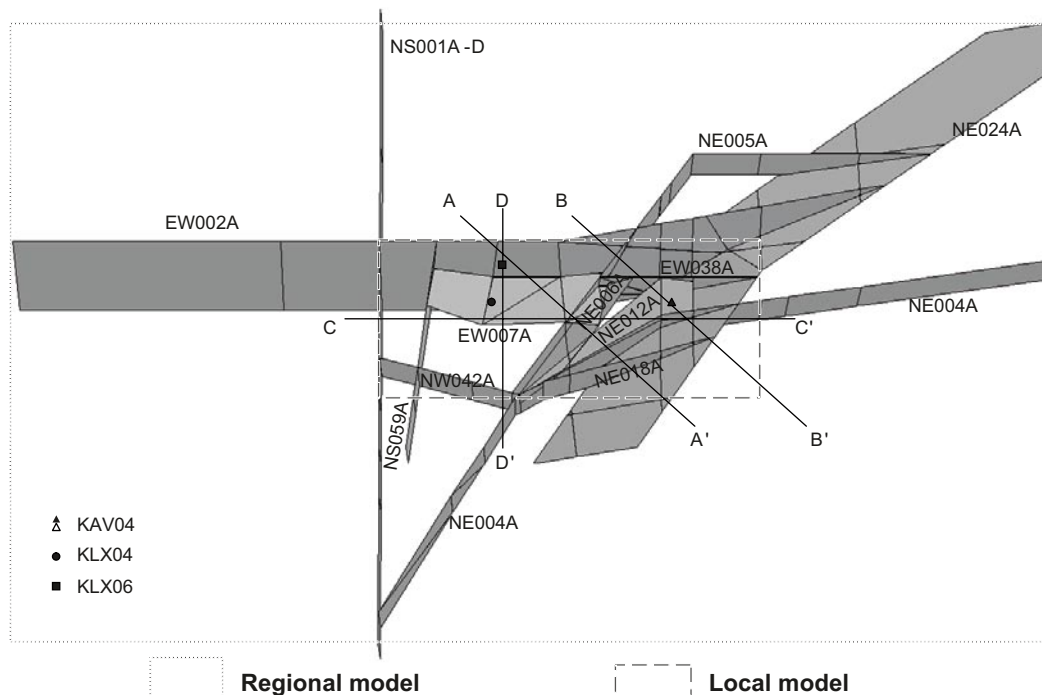


Figure 3-2. Deformation zones modelled by 3DEC and reference sections. The EE' section (not shown) runs parallel and close to DD' intersecting KLX04.

Table 3-1. Coordinates used for regional and local models.

Model	Coordinates
Regional model	(1560000, 6373000), (1560000, 6360000), (1539000, 6360000), (1539000, 6373000) from top right corner in clock-wise direction
Local model	(1554100, 6368200), (1554100, 6365000), (1546400, 6365000), (1546400, 6368200) from top right corner in clock-wise direction

Table 3-2. Deformation zones intersecting the Laxemar local model volume.

Deformation Zone	Measured orientation strike/dip	Width/Length	Modelled orientation strike/dip	Note
ZSMNS001A,B,C,D	10±15 / 90±15	100±50 m / > 11 km	0/90	A, B, C and D are connected.
ZSMEW002A (Mederhult)	90±20 / 65±10	100 m (20–200) / 17.9±5 km	90/65, 80/65	Cut by ZSMNE024A
ZSMNE004A	50±20 / 90±20	100 m (20–120) / 15.7 km (8–15)	82/90, 60/90, 32/90	Strike 82 from the aerial map.
ZSMNE005A (Äspö shear zone)	60±30 / 90±10	250 m (50–300) / 10.5±0.2 km	36.7/90, 90/90	Strike 36.7 from the aerial map. Cut by ZSMNW042A in the bottom.
ZSMNE006A	215±10 / 65±20	130 m (60–130) / 2.1 km (2–4)	215/65	Cut by ZSMEW038A & ZSMNE005A
ZSMEW007A	278±20 / 43±10	50 m (20–60) / 3.2±0.2 km	270/43, 290/43	Cut by ZSMEW002A, ZSMNS059A & ZSMNE006A
ZSMNS009A	10±10 / 90±15	80±40 m / 10 km (10–12)	x	Does not reach local model.
ZSMEW009A	85±15 / 76±10	12 m (5–20) / 1.8±0.1 km	90/90	Merged with ZSMEW038A.
ZSMNE010A	55±15 / 90 (?)	10 m (2–10) / 3.4±0.2 km	x	Width less than 50 m.
ZSMNE011A	55±15 / 90 (?)	100±50 m / 8.6 km (8–12)	x	Width less than 50 m.
ZSMNE012A	60 (50–110) / 45±10	120 m (60–120) / 5.5±0.2 km	50/45	Cut by ZSMEW004A (GEO1) Cut by ZSMNE018A & ZSMNE024A (GEO2)
ZSMEW013A	85 (105–65) / 90±10	45 m (20–50) / 4.4 km (2.5–4.4)	x	Width less than 50 m
ZSMNE015A	50±20 / 70±10	10 m (3–15) / 1.9±0.2 km	x	Width less than 50 m
ZSMNE015B	80±10 / 90±10	5 m (1–5) / 1.0 km±0.1 km	x	Width less than 50 m
ZSMNE016A	30±20 / 90±10	15±10 m / 1.4±0.1 km	x	Width less than 50 m
ZSMNS017AB	335±10 / 83±10	20 m (20–100) / 1.0±0.1 km	x	Width less than 50 m
ZSMNE018A	80±10 / 90±10	50±25 m / 1.2±0.1 km	75/90	Cut by ZSMEW004A & ZSMNE024A
ZSMNE019A	60±15 / 90±20	5 m (1–10) / 3.7±0.2 km	x	Width less than 50 m
ZSMEW023A	275±15 / 90±20	20 m (5–50) / 3.8±0.2 km	x	Width less than 50 m
ZSMNE024A	225±10 / 52±10	80 m / 11.7 km (10–15)	235/52, 215/52	
ZSMNW025A	110±10 / 90±10	10 m (1–15) / 1.9±0.1 km	x	Width less than 50 m
ZSMNW028A	105±15 / 90±10	10±5 m / 1.1±0.1 km	x	Width less than 50 m
ZSMNE031A	215±20 / 52±20	15 m (2–20) / 4.5 km (4–15)	215/52	Merged with ZSMNE024A.
ZSMEW038A	90±10 / 90±15	10 m (1–15) / 3.2±0.1 km	90/90	Merged with ZSMEW009A.
ZSMNE040	30±10 / 90±10	20 m (5–20) / 1.4±0.1 km	x	Width less than 50 m.
ZSMNW042A	105±10 / 90±20	80 m (30–80) / 3.4±0.1 km	105/90	Cut by ZSMNE004A
ZSMNE050A	45 (35–65) / 90±15	50 m (20–70) / 2.2 km (2–3)	32/90	Merged with ZSMNE004A
ZSMNS059A	00±10 / 90±10	50 m (20–60) / 5.4±0.2 km	08/90	
ZSMEW900A	100±20 / 70±20	20±10 m / 1.6 km (1–2)	x	Width less than 50 m
ZSMNW929A	113±10 / 79±20	50 m (20–50) / 1.9±0.2 km	x	Width marginally passed the limit but maximum still 50 m.
ZSMNE930A	65±10 / 90±10	5 m (1–30) / 4.2±0.2 km	x	Width less than 50 m
ZSMNW931A	165±10 / 90±15	50 m (50–100) / 3.9±0.2 km	x	Influence is expected to be little.
ZSMNW932A	120 (120–90) / 90±20	0 m (0–20) / 2.9±0.2 km	x	Width less than 50 m
ZSMNW933A	150 (150–90) / 90±15	40± 20 m / 3.8±0.2 km	x	Width less than 50 m

Figure 3-3 shows sections taken through the model. Two geometrical models were considered in this study; “base geometry” (GEO1) and “alternative geometry” (GEO2). The difference between the two cases is about the way the deformation zone ZSMNE012A is terminated. ZSMNE012A is terminated against ZSMNE004 in GEO1 while it is terminated against ZSMNE018A and ZSMNE024A in GEO2.

Figure 3-4 shows horizontal section views of the geometry within the local model. The view changes depending on the depth as the deformation zones are not all vertical. For example, deformation zone ZSMEW002A appears inside the local model with the increasing depth while ZSMEW007A moves toward the upper boundary of local model.

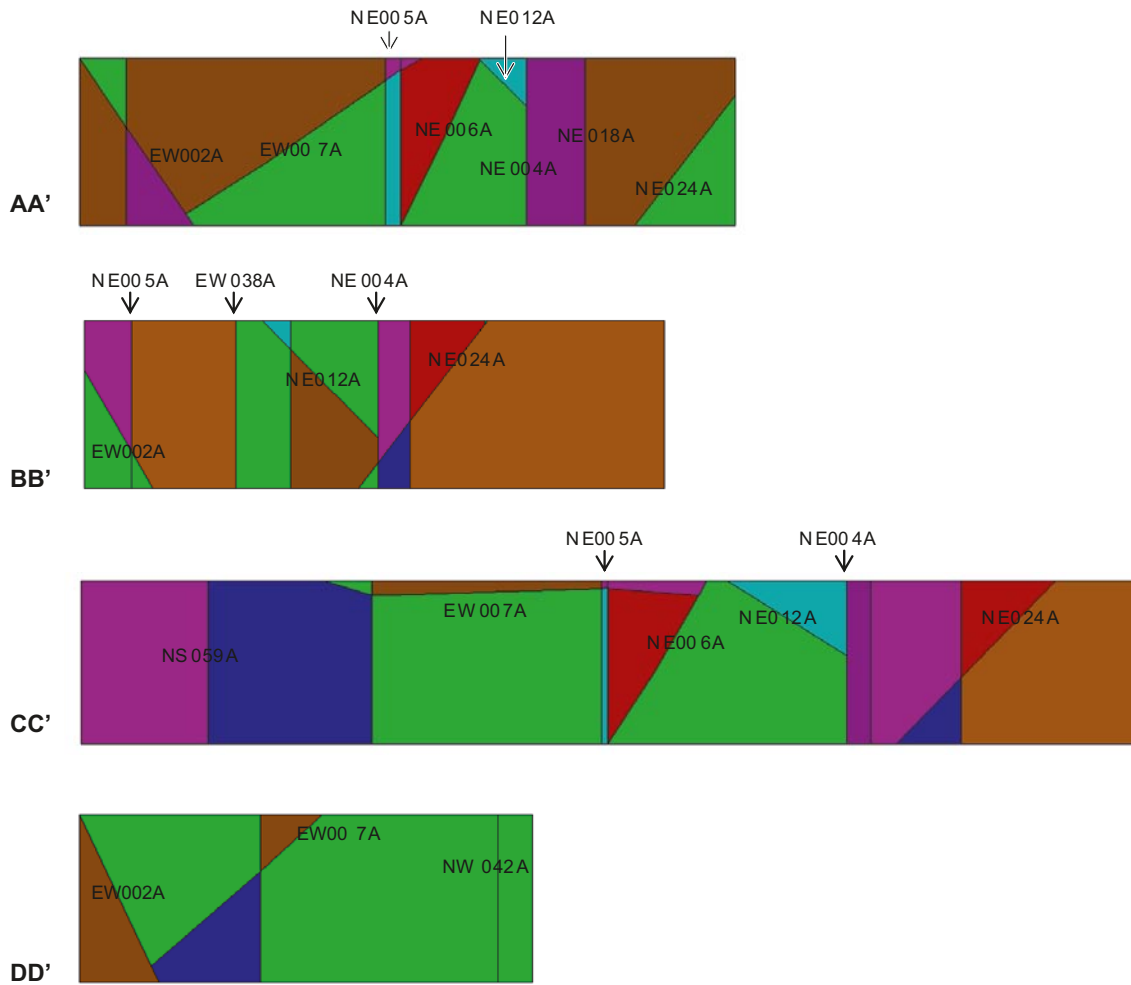


Figure 3-3. Vertical section views of the local model in 3DEC, with the included deformation zone discontinuities marked. The locations of sections are given in Figure 3-2.

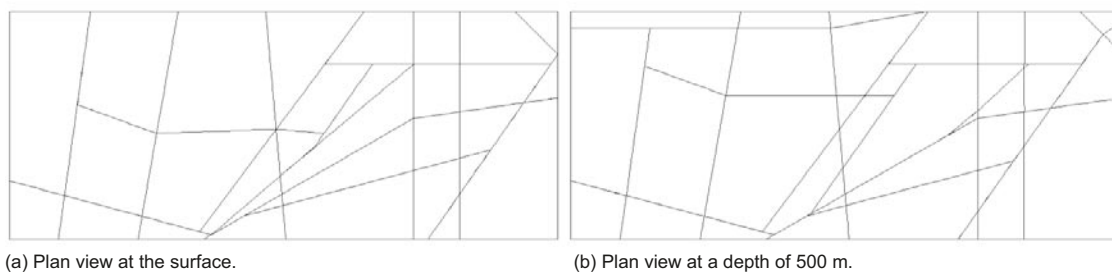


Figure 3-4. Plan view of the generated discontinuity planes (deformation zone geometry) within the local model; Compare with the mapped structures in Figure 3-5.

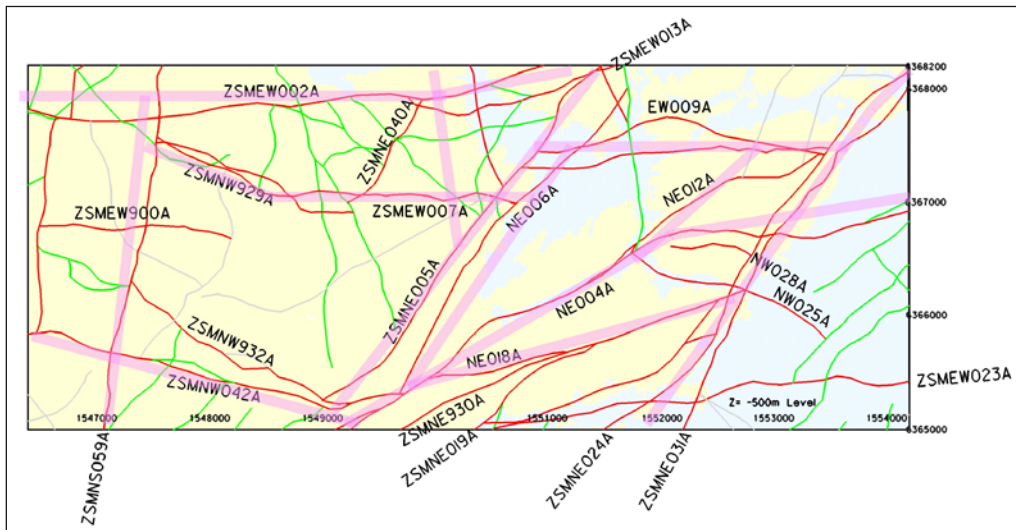


Figure 3-5. Deformation zone model Laxemar 1.2 at 500 m depth. The discontinuity planes in the 3DEC model are shown in pink.

3.3 Numerical model size and boundary conditions

Figure 3-6 presents the geometry of the numerical model with boundary stress conditions. The side edge lengths of the model are 40 km and the depth of the model is 4 km. The NE-SW vertical sides of the model were set perpendicular to the general direction (selected based on previous stress model version) of the major principal stress. The so called “regional model volume” which includes the “local model volume” lies in the centre of the numerical grid. The boundary stresses were applied with a gradient so that the gradual increase of stress with the depth could be modelled. The top plane, representing the ground surface was free from any restraints and the bottom of the model was hindered to displace in the vertical direction.

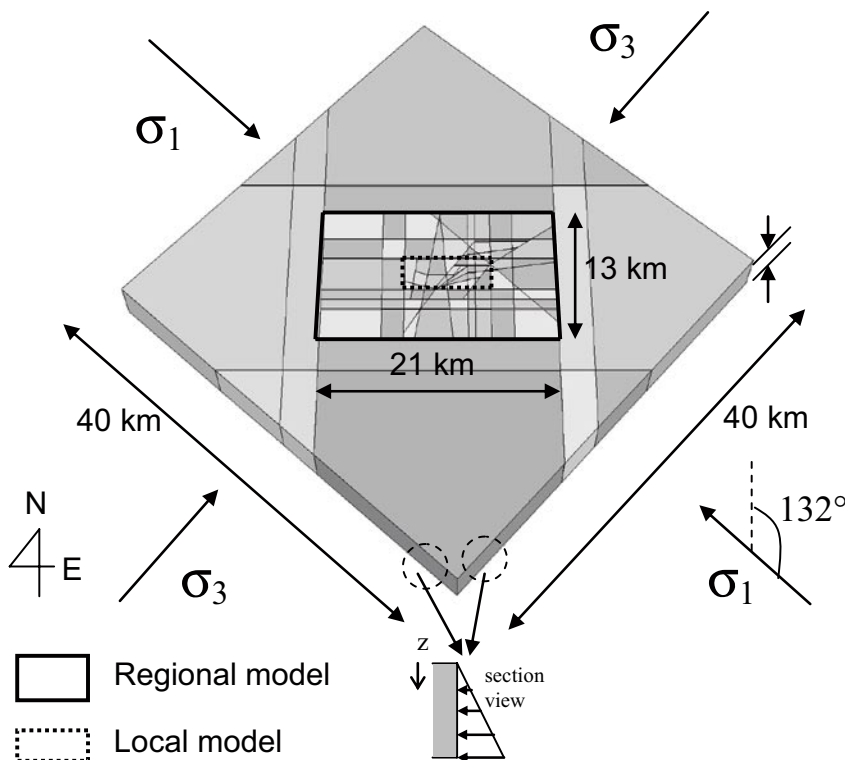


Figure 3-6. Geometry of Laxemar area modelled by 3DEC.

Horizontal stresses were applied to the vertical sides of the numerical model. Vertical loads corresponding to gravitational forces are also simulated in the model. The measured in situ stress data showed that the ratio between the horizontal to vertical stresses varies between three and four and the vertical stress tends to be the intermediate principal stress. To enable the effect of different assumed stress states in the model, three different cases for the stress assumed at the boundaries were included in this study. The cases are denoted LSM1-LSM3 (Laxemar Stress Model 1-3). The cases have a different gradient with depth for the maximum (σ_1) and the minimum (σ_3) principal stresses, as shown in Figure 3-7. The intermediate principal stress is assumed vertical and equal to the weight of overburden in all three model cases. LSM3 has the largest stress magnitudes and the ratio between maximum and minimum principal stresses while LSM2 has the lowest magnitude and lowest stress ratio. Hence, LSM3 is expected to provide a condition where more slip on deformation zones takes place.

Figure 3-8 shows the model block discretized and meshed. Finer meshes were used in the regions of the interest and coarser meshes were used outside of the regional model. The maximum edge length of a tetrahedron in the outer model is 2 km and this gradually decreased to 100 m in the centre of the model.

3.4 Mechanical properties of the numerical model

Boundary stresses and mechanical properties of the rock mass and the deformation zones used in this study are listed in Table 3-3. The Young's modulus and Poisson's ratio of the rock mass from the site investigation for Simpevarp, /SKB 2004/ are given in Table 3-3. Friction angle is the most important single parameter when the influence of deformation zones is considered. Friction angles used for this study are inferred from the existing data on deformation zones and fractures. Friction angle of a single fracture ranges from 30 to 40 degrees. Empirical studies suggest that the friction angle of the deformation zones are in the order of 40 degrees. In this study, a reduced value, 20 was used as a base study and additional cases with 15 and 25 degrees were also considered as parametric studies. This reduction is justified due to the fact that:

- 1) the sliding of joint is subject to the orientation while failure of deformation zone is not, i.e. direct use of friction angle for continuous deformation zone does not ensure any failure along the planar joint,
- 2) the weakest part of deformation zone, which may have triggered the failure of deformation zone, will have much lower friction angle.

In fact, due to the clay content in a deformation zone, there is a possibility that the friction angle of the deformation zone is much lower than 40 degrees. The friction angle of soils rich in clay can be as low as a few degrees. More detailed analysis as how to select friction angle for modelling the deformation zones are presented in the section for uncertainty analysis.

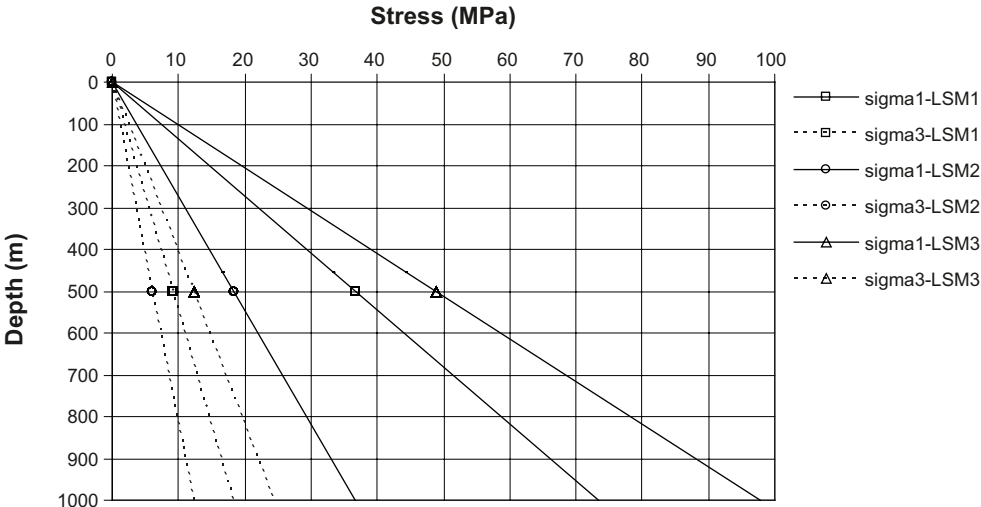
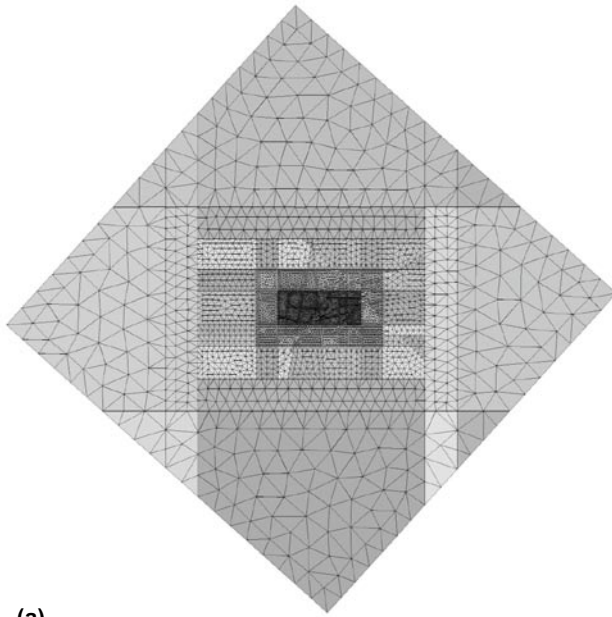
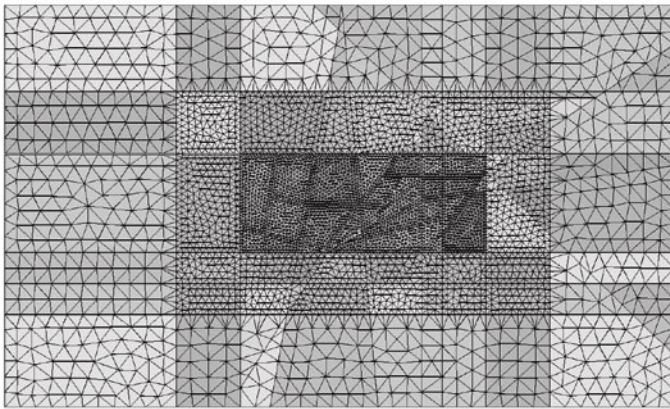


Figure 3-7. Three different stress models (Laxemar Stress Model) used in the numerical modelling; Note that the initial intermediate principal stress was assumed vertical and equal to weight of overburden. See also Table 3-3.



(a)



(b)

Figure 3-8. Generated meshes for (a) entire model, (b) regional model. The maximum length of a tetrahedron in the local model was 100 m.

Table 3-3. Stress boundary conditions and mechanical parameters used for the study.

	LSM1	LSM2	LSM3	
Maximum Principal stress, σ_1 (MPa)	0.074z (3 × $\rho g z$)	0.037z (3/2 × $\rho g z$)	0.098z (4 × $\rho g z$)	ρ : density of rock g : gravitational acceleration z : depth
Intermediate Principal stress, σ_2 (MPa)	0.025z ($\rho g z$)	0.025z ($\rho g z$)	0.025z ($\rho g z$)	
Minimum Principal stress, σ_3 (MPa)	0.018z (3/4 × $\rho g z$)	0.012z (1/2 × $\rho g z$)	0.025z ($\rho g z$)	
Rock mass Modulus of Deformation (GPa)	40	40	40	Mean of domain A /SKB 2004/
Poisson's ratio	0.15	0.15	0.15	Mean of domain A /SKB 2004/
Friction angle (1)	20°	20°	20°	Except Zone NS001A. 15° and 25° were also used for sensitivity study.
Friction angle (2)	35°	35°	35°	Zone NS001A-D (higher property to consider discontinuity)
Normal Stiffness (1) (GPa/m)	1	1	1	Except zone NS001A
Normal Stiffness (2) (GPa/m)	10	10	10	Zone NS001A
Shear Stiffness (1) (GPa/m)	1	1	1	Except Zone NS001A
Shear Stiffness (2) (GPa/m)	10	10	10	Zone NS001A

Normal stiffness of a planar joint representing a deformation zone was taken to be 1 GPa/m. This value was determined by estimating the load-induced contraction of a deformation zone having a width of 50 m. Shear stiffness of the planar joint was assumed to be identical with the normal stiffness. In order to consider the simplification of deformation zone NS001A-D, consisting of several shorter non-aligned segment, higher friction angle and stiffness were assigned for this deformation zone as sliding along this deformation zone is not expected.

3.5 Stress distribution in vertical and horizontal sections

Figure 3-9 presents the shear displacement across the deformation zones, shown on vertical and horizontal sections in the local model. Deformation zones ZSMEW002A, ZSMEW007A and ZSMNE024A have the largest displacements and their corresponding impact on the stress distribution should be underlined. In general near vertical deformation zones do not produce large displacement across their surfaces due to the stress direction with respect to the orientation of those zones. Displacement across the vertical deformation zone ZSMEW038A and the upper part of zone ZSMNE004A are larger than displacements across the other vertical deformation zones as their orientations are more unfavourable for the sliding. This reconfirms the importance of the orientation of the deformation zones in relation to prevailing in situ stress field.

Figure 3-10 presents the variation in principal stresses along vertical sections AA', BB' and CC' for Case LSM3. The results plotted cover the entire length of the regional model. Boundary stress magnitudes are also added for a comparison. Note that the boundary stresses for the intermediate and the minimum principal stresses are the same for the case LSM3. Variation of stresses seen is due to the influence of deformation zones and their interaction. In general, the maximum principal stress decreases and intermediate and minimum principal stresses increase or do not change significantly in wedge-shaped blocks confined by the deformation zones.

In section AA', a distinct decrease of stress is observed in two locations. Decrease occurs at a wedge-shaped block formed by deformation zones ZSMEW002A and ZSMEW007A and also near the deformation zone ZSMNE024A. Between these two locations, a slight increase of intermediate principal stress is observed, which is caused by the stress equilibrium in the model. In section BB', there is an overall decrease of maximum principal stress. In this section a big wedge formed by the deformation zone ZSMEW002A and ZSMNE024A can explain this trend of the stresses. In section CC', more fluctuation of stress is observed. Especially near the x-coordinate 52,000 m an unusually high stress concentration is observed, due to the small wedge formed by the zones ZSMNE012A and ZSMNE004A. As this may be due to a lock-up of a wedge, additional analysis with alternative geometry (GEO2) was performed, see under Section 3.6.

Figure 3-11 presents similar sections as in Figure 3-10 for a depth of 250 m. In general similar trends, though with less magnitudes in the variations can be observed at this depth.

Figure 3-12 presents the orientation (trend) of the principal stresses in the same vertical sections, along horizontal lines at 450 m depth. As with the stress magnitudes, the stress orientation also changes due to the deformation zone. Detailed analyses are needed in order to include the change of dip angle of the principal stresses.

Figure 3-13 shows the distribution of the principal stresses across section AA'. Both the direction and the magnitude of the stresses are much influenced by the existence of deformation zones in the model.

Figure 3-14 presents the variation in principal stresses for the models LSM1 and LSM2 along section AA'. The results from Model LSM1 are similar to those from Model LSM3. However, there is a very little variation in stresses for Model LSM2.

Figure 3-15 presents the stress distribution in horizontal section, at two different depths, through the local model. At the depth of 50 m, there is a clear influence of deformation zones on the orientation of principal stresses. This is because the shallow overburden can not offer large normal stresses on the deformation zones to hinder the shear displacements. Stress concentrations are found in the mid-south and south-west of the local model due to the abrupt termination of the deformation zones as modelled. It is not known whether or not the natural deformation zones have such an abrupt termination.

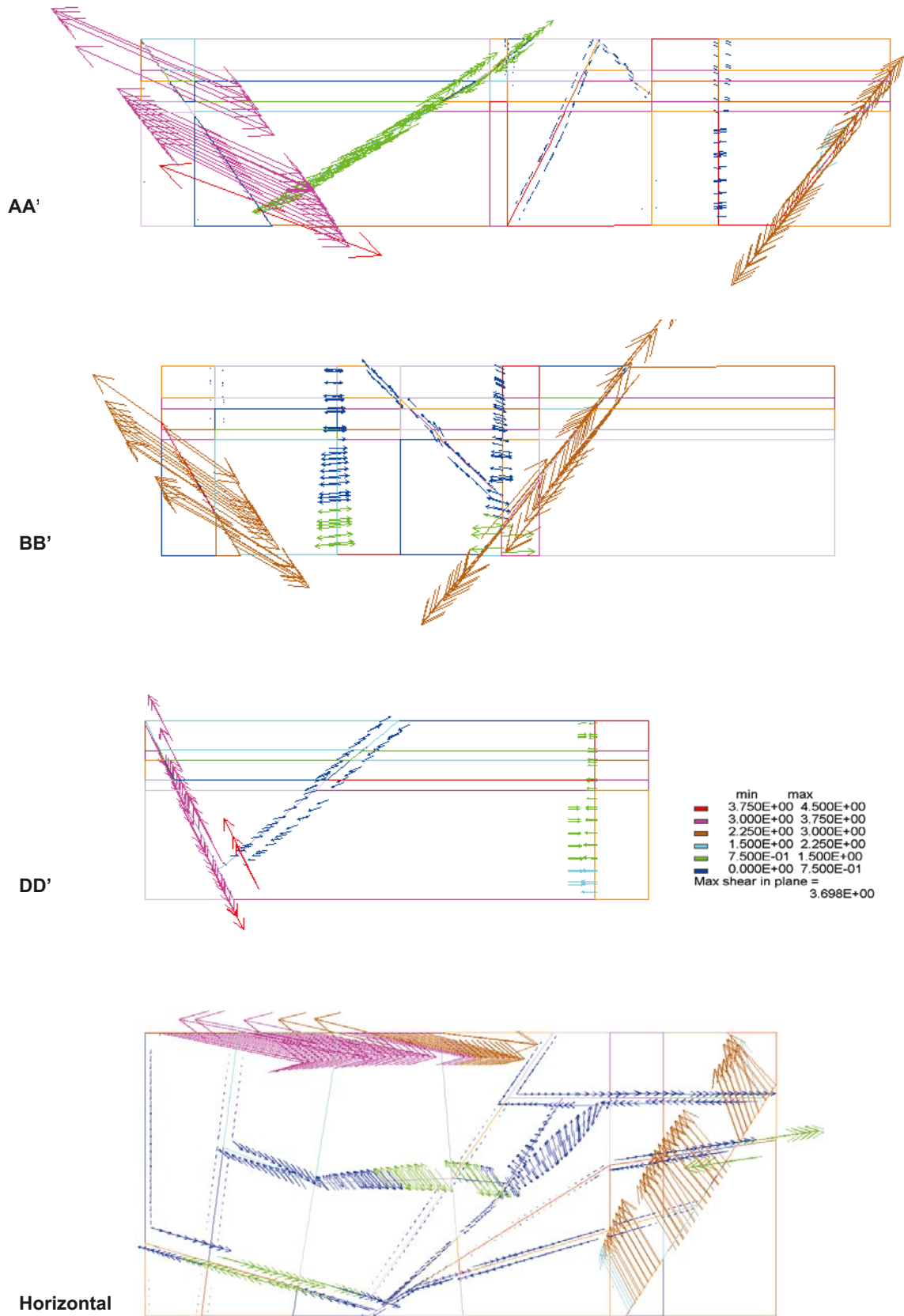


Figure 3-9. Shear displacement of deformation zones within the local model shown on vertical and horizontal sections. (For geometry case GEO1 and stress case LSM3).

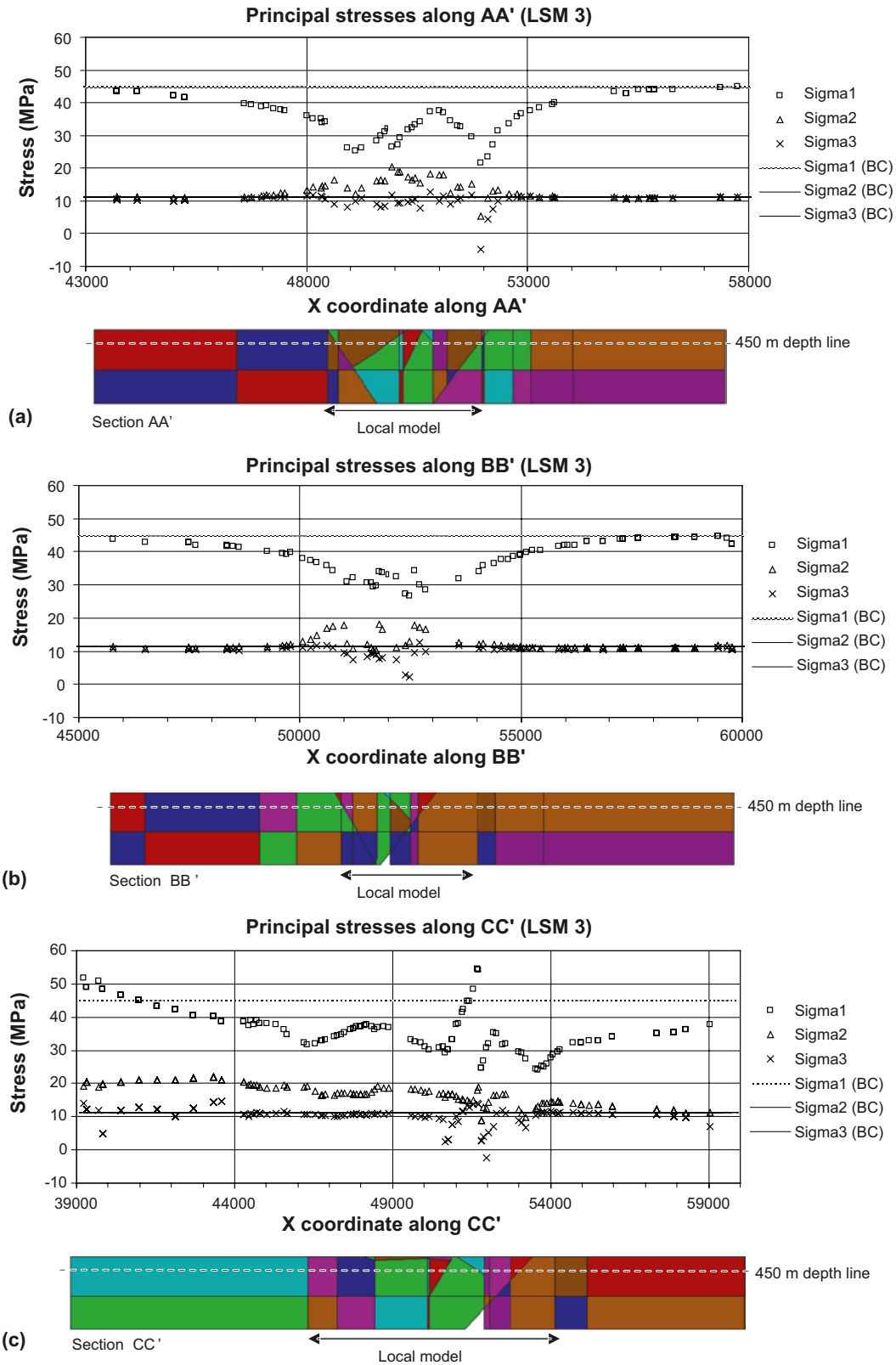


Figure 3-10. Principal stresses along reference lines at 450 m depth (LSM3); (a) section AA', (b) section BB', (c) section CC'. Note the identical scale of the graphs and the sections. (The locations of the sections are shown in Figure 3-5 and boundary conditions for LSM1-3 given in Table 3-3).

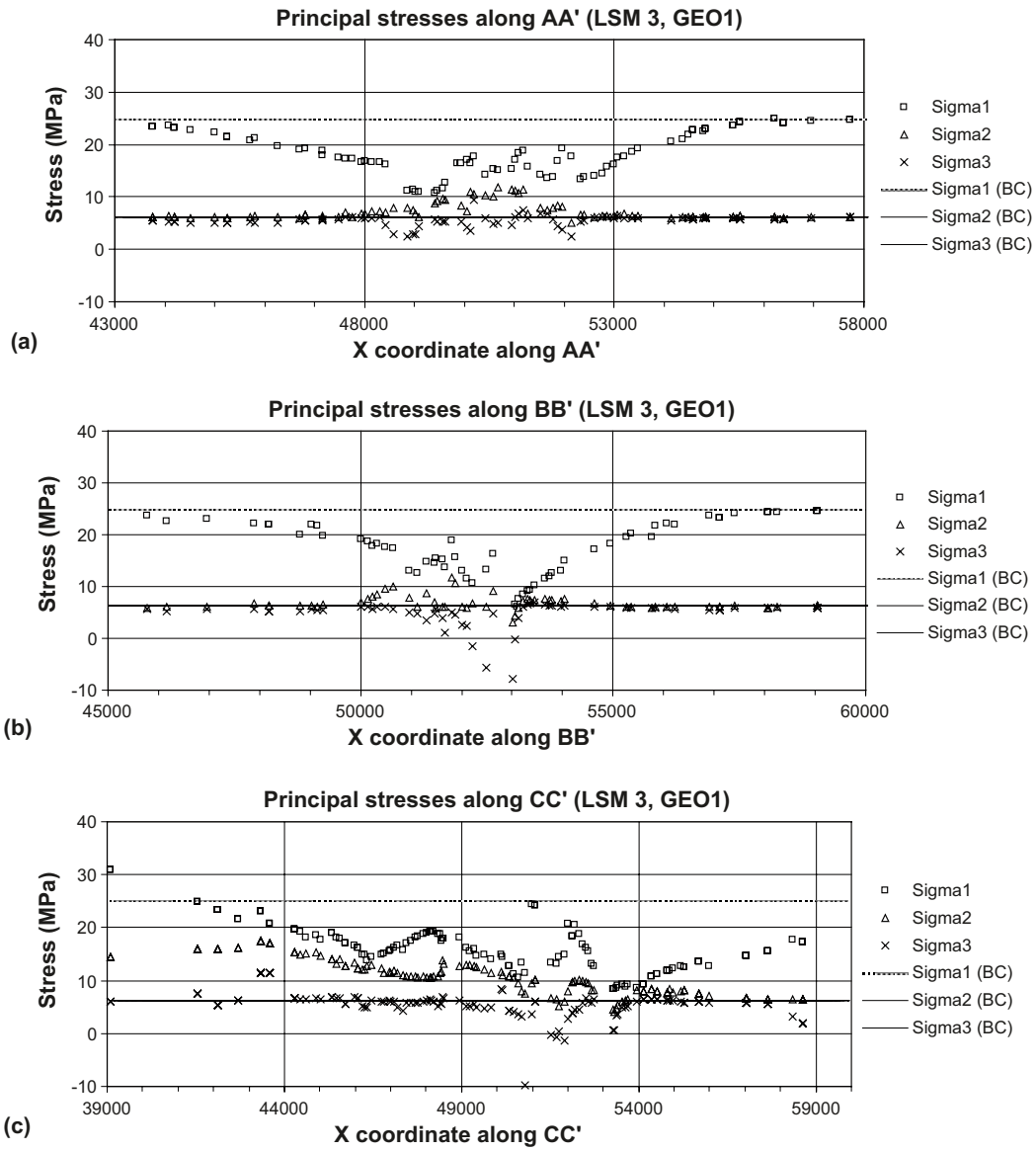


Figure 3-11. Principal stresses along reference lines at 250 m depth (LSM3); (a) section AA', (b) section BB', (c) section CC'. (The locations of the sections are shown in Figure 3-5 and boundary conditions for LSM1-3 given in Table 3-3).

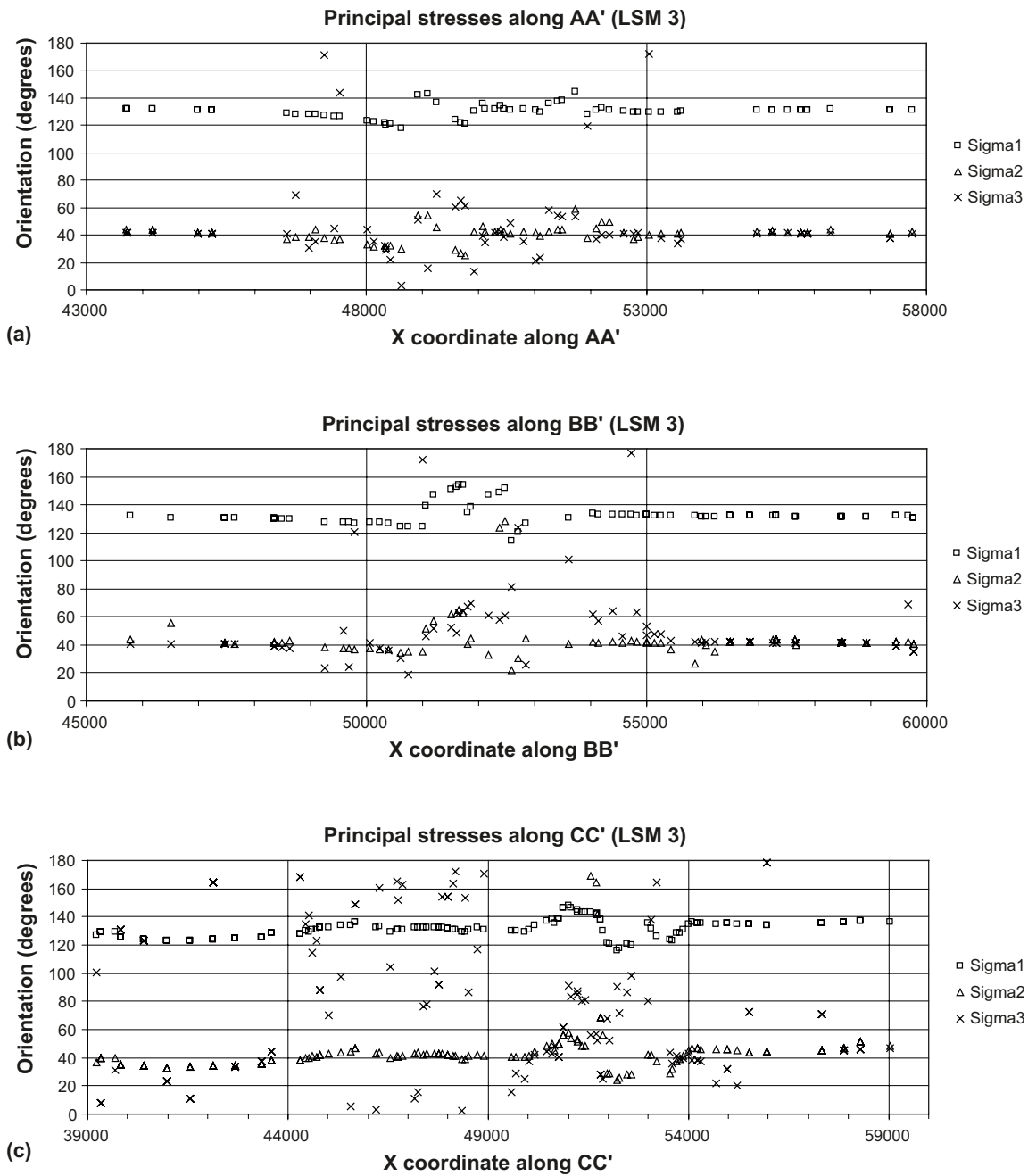


Figure 3-12. Orientation (trend) of principal stresses along reference sections at 450 m depth (LSM3); (a) section AA', (b) section BB', (c) section CC'. Orientations are measured from the North axis. (The locations of the sections are shown in Figure 3-5 and boundary conditions for LSM1-3 given in Table 3-3).

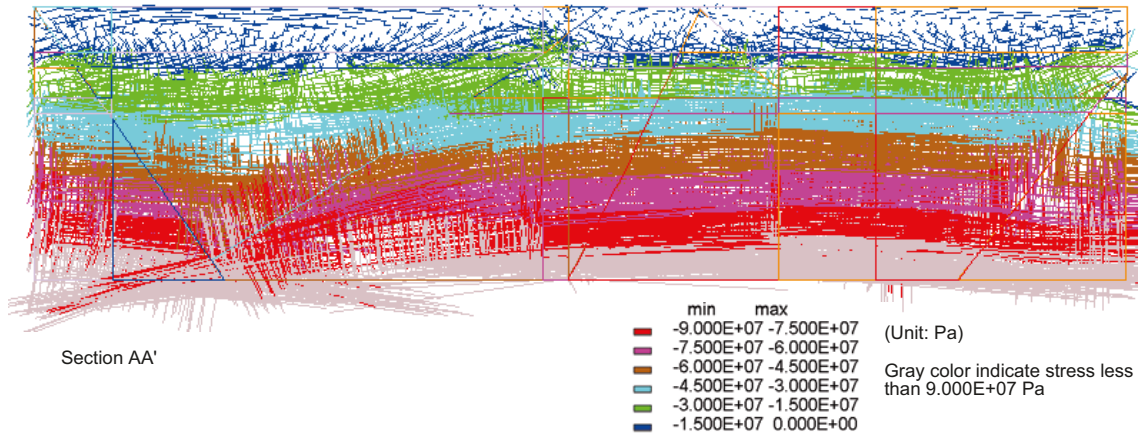


Figure 3-13. Distribution of principal stresses across reference section AA' (LSM3).

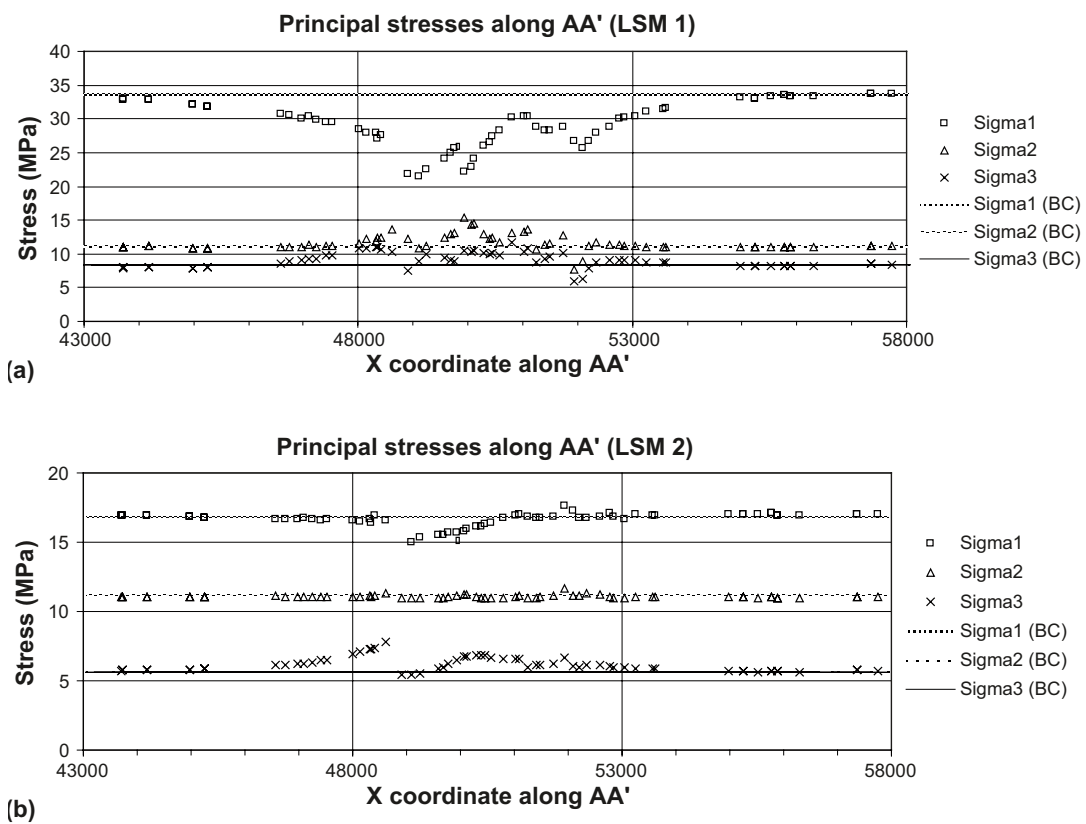


Figure 3-14. Principal stresses along reference sections at 450 m depth; (a) LSM1, (b) LSM2.

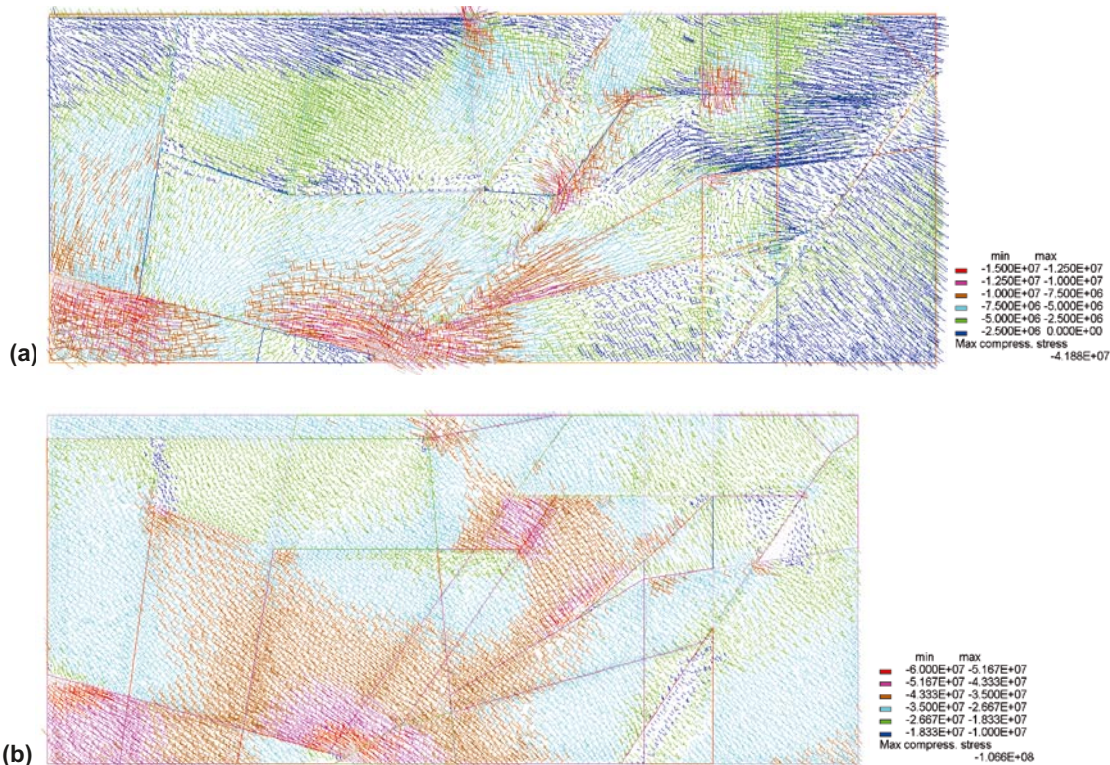


Figure 3-15. Principal stress distribution on horizontal sections through the local model (LSM3); (a) 50 m depth, (b) 450 m depth.

At 450 m depth the stress magnitudes, shown as different colours in the figure, varies within the area, while the changes in orientation is less. (Note that the colour legend is not the same between the two depth figures.) The span in magnitude between the areas with highest and lowest maximum principal stress is from about 20 MPa to 50 MPa, for this case (LSM3).

3.6 Comparison between measured and modelled in situ stresses

Comparisons are made between measured and modelled stress in boreholes KLX04, KAV04A and at Äspö.

3.6.1 Comparison in borehole KLX04

Borehole KLX04 is located in the mid-West of the local model (Figure 3-2). Rock stress was measured by overcoring method in this borehole. The deformation zone ZSMEW007A intersects the borehole KLX04 between 314 m to 391 m borehole depth (geometrical intercept). Figure 3-16 shows the stress distribution at section EE' for the three numerical model cases (LSM 1, 2 and 3). Section EE' passes through the KLX04. A clear influence of the deformation zone ZSMEW007A can be observed in the models LSM1 and LSM3. In LSM2, the effect of deformation zone is not noticeable since no sliding occurred across the deformation zone and therefore no redistribution of stresses took place. In models LSM1 and LSM3, the wedge formed by ZSMEW007A and ZSMEW002A is partially de-stressed. This distinct change in stress magnitudes is clearer for LSM3 than for LSM1. This is because in the LSM3 the sliding criteria were reached in earlier stages, resulting in greater perturbation in the stress field.

Figure 3-17 presents a comparison between the measured and the modelled stresses at KLX04. Measured stresses show a distinct increase of stress for maximum and intermediate principal stresses at about the depth of the intersection of the deformation zone ZSMEW007A (at about 320m vertical depth). This is explained by the effect of the deformation zone. Of the three stress models, LSM3 matches best with

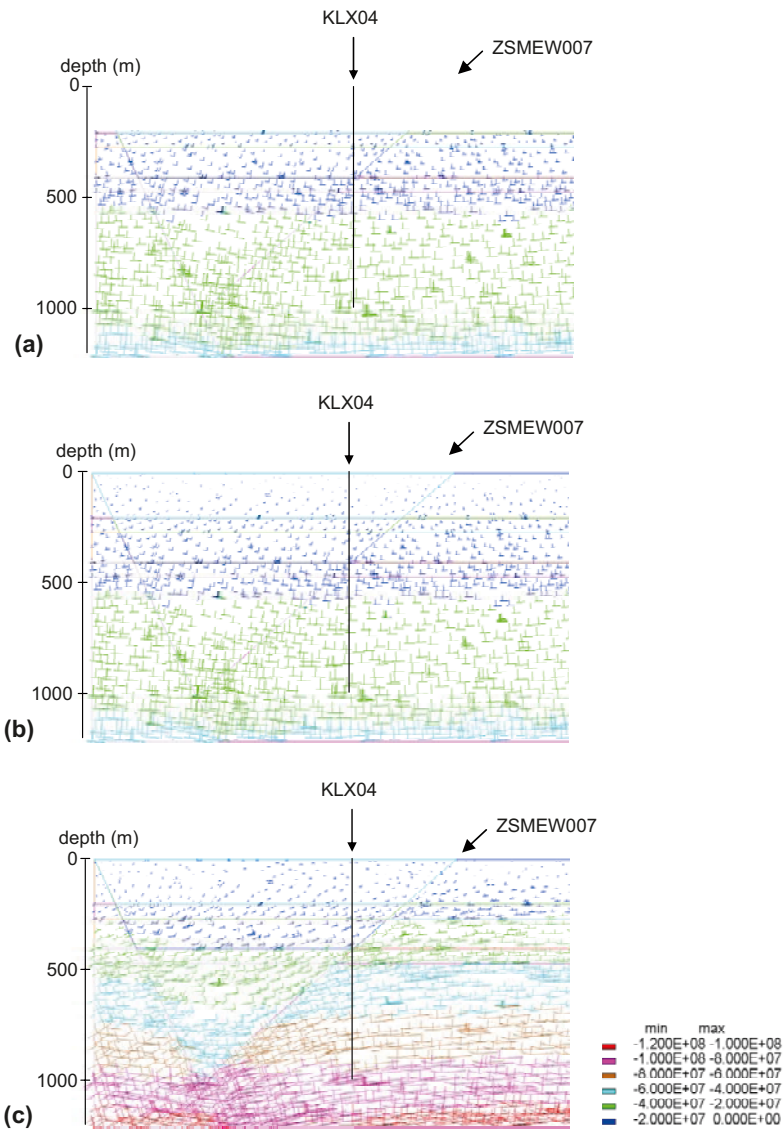


Figure 3-16. Stress distribution at Section EE' through KLX04; Stress model case (a) LSM1, (b) LSM2, (c) LSM3.

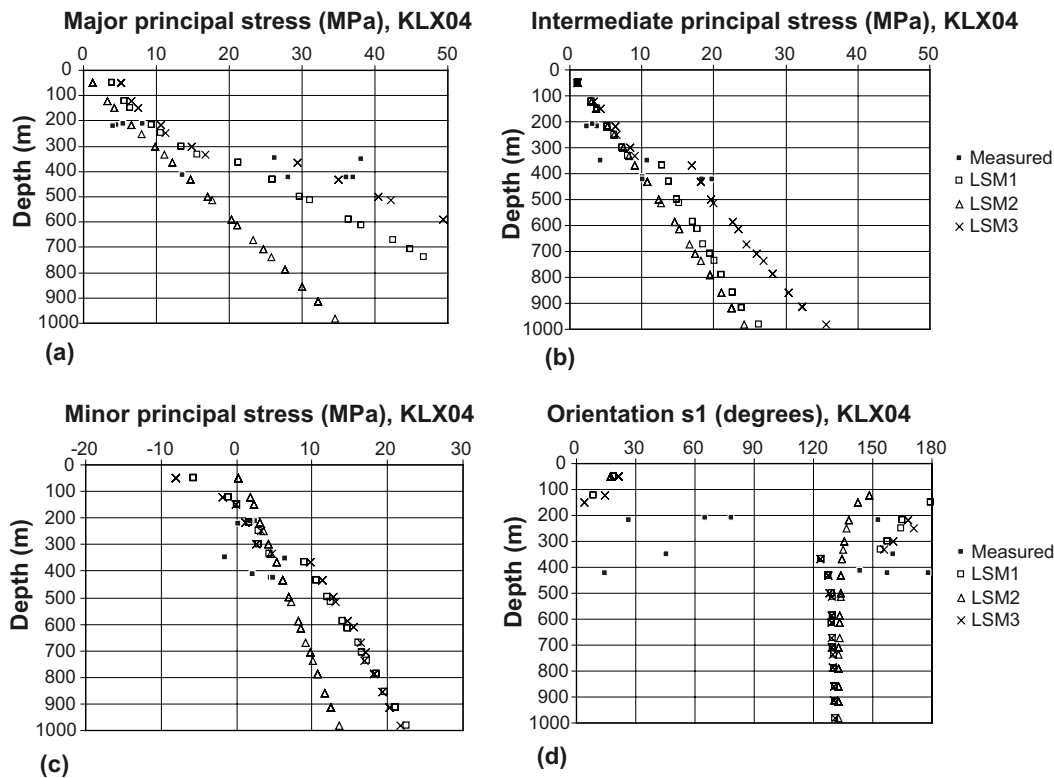


Figure 3-17. Comparison between measured and modelled stress at KLX04; (a) Major principal stress, (b) Intermediate principal stress, (c) Minor principal stress, (d) orientation of major principal stress from north axis.

the measured results. The orientation presented in Figure 3-17d is the trend of maximum principal stress (in cases the trend was larger than 180 degrees, 180 degrees are subtracted). Direct comparison with the numerical model results is difficult because of the scatter in measured stresses. Modelled stresses show that rotation of stress direction occurs at the intersection of the deformation zone.

3.6.2 Comparison in borehole KAV04A

Borehole KAV04A is located in the mid-East of the local model (Figure 3-2) and rock stress was measured by overcoring method. The borehole intersects the deformation zone ZSMNE012A between 745 m and 947 m borehole depth (geometrical intercept). In situ stress was measured in borehole KAV04A, above the intersection of the deformation zone. Figure 3-18 shows the modelled stress distribution across section BB'. In general, the influence of the deformation zone ZSMNE012A is not clearly evident. On the other hand, the vertical deformation zone ZSMNE004A seems to have affected the stress distribution. The direction of the movement of ZSMNE004A can be seen in Figure 3-9.

Figure 3-19 shows the comparison between measured and modelled stress at KAV04A for the three different stress models. Models LSM1 and LSM3 generally overestimate the stress while LSM2 fits better to the in situ measurements. This is mainly because the applied boundary stress is lower in LSM2 than for the other two models. The orientation of measured stress is also more scattered compared with that of the modelled stress.

3.6.3 Comparison in Borehole KLX02

The borehole KLX02 is located just north of the deformation zone ZSMEW007 in the centre of the Laxemar local volume. In this borehole measurements with hydraulic fracturing were performed by /Ljunggren and Klasson 1997/. The hydraulic measurements results may be compared to the modelling results from the minimum horizontal stress, since this method is expected to give a fairly good result on this parameter. The comparison for magnitude and orientation is presented in Figure 3-20 and Figure 3-21, respectively.

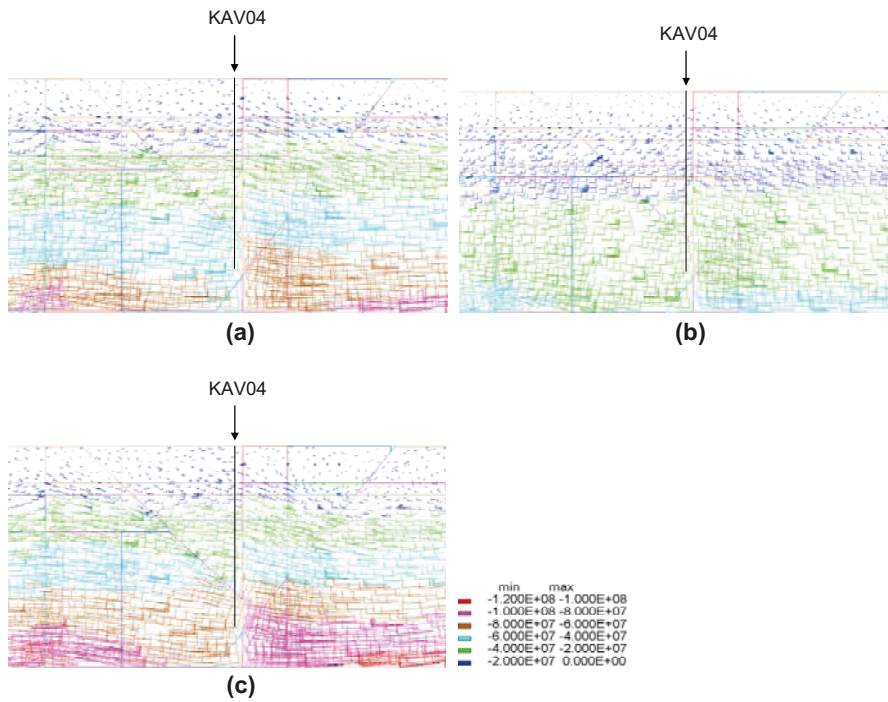


Figure 3-18. Modelled stress distribution at KAV04A; (a) LSM1, (b) LSM2, (c) LSM3.

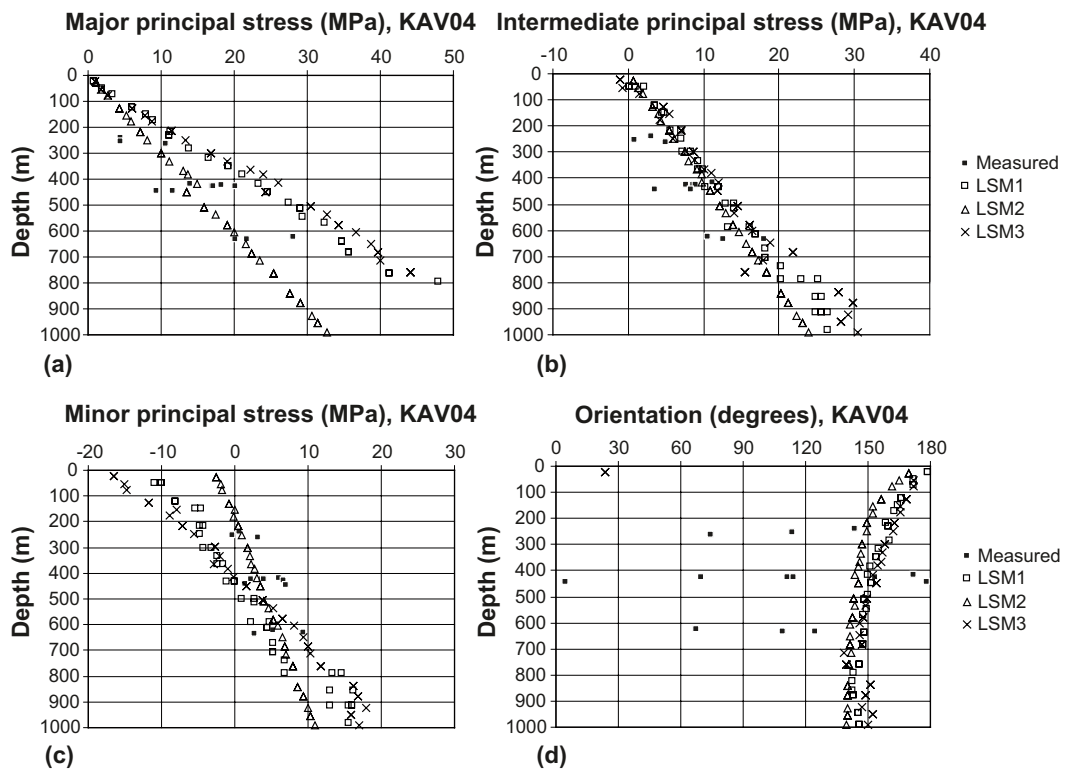


Figure 3-19. Comparison between measured and modelled stress at KAV04A; (a) Major principal stress, (b) Intermediate principal stress, (c) Minor principal stress, (d) orientation of major principal stress.

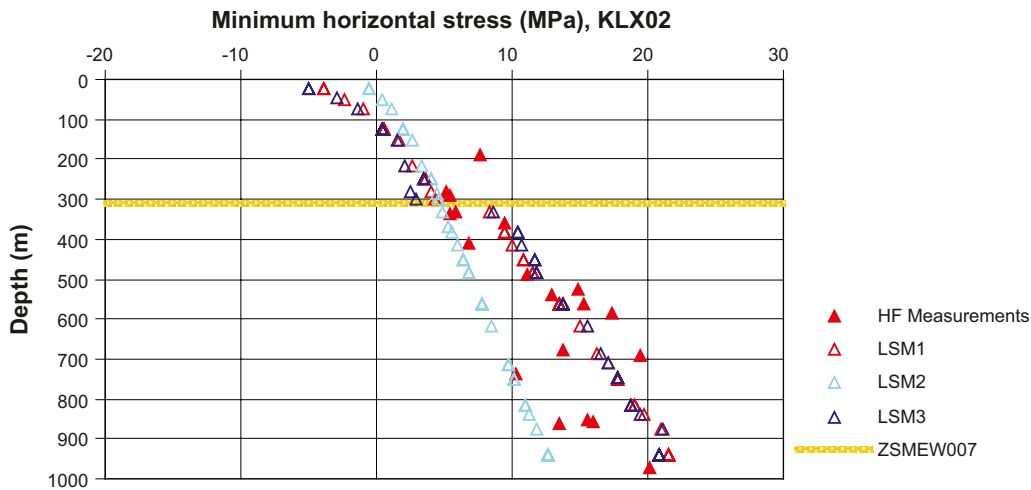


Figure 3-20. Comparison between measured and modelled stress at borehole KLX02, minimum horizontal stress. KLX02 is located at central Laxemar starting above the deformation zone ZSMEW007 while most measurements are from below the zone.

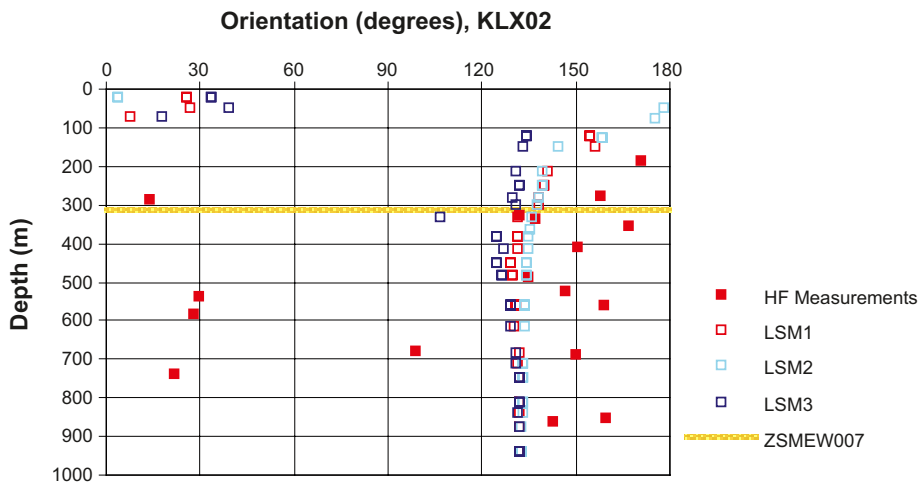


Figure 3-21. Comparison between measured and modelled orientation of major principal stress at borehole KLX02, for the three different stress model cases.

Since this borehole passes through the interpreted deformation zone ZSMEW007, the influence of this zone on the model may also be noted in the figures. (The location of the zone intersection with borehole in the model and the borehole may differ slightly since the model is only a simplification of the real geometry.) The measurements are unfortunately, with one exception located at, or below, this deformation zone. This means that the results from the measurements can not be used to confirm the stress decrease seen from the models, but can be used for the domain below the deformation zone.

Both the magnitude and orientation of the stress varies fairly much in the measurements but there is an indication of an orientation in the range 130–160°, and magnitudes are similar to stress model LSM1 and LSM3. Some of the data that are more far from the model in terms of magnitude are also more off in terms of orientations.

3.6.4 Comparison with the Äspö area

The Äspö Hard Rock Laboratory is located in the northern part of the local model. A number of stress measurements were conducted in the area using both overcoring and hydraulic fracturing methods. Within the depth considered in this study (< 1,000 m), the rock volume around the laboratory is not

intercepted by what in this modelling context is considered as a large regional deformation zone (Section 3.2).

Figure 3-22 presents the comparison between measured and modelled stresses at the Äspö area. Even though the direct comparison is not easy due to the scattering of the measured stresses, LSM1 and LSM3 seem to lie in the middle of the scatter of the measured stresses.

From the comparisons on borehole KLX04, KAV04A, KLX02 and the Äspö area, LSM3 is closest to the measured stress and calls for further investigations as given below.

3.7 Effect of friction angle

Effect of friction angle across a deformation zone is investigated by changing the angle between 15 and 25 degrees. Figure 3-23 shows the stress distribution with friction angles 15, 20 and 25 degrees. The plots clearly indicate that the smaller friction angles facilitate the slip across a deformation zone, and that the stress results therefore are fairly sensitive to this parameter.

3.8 Effect of change in zone ZSMNE012A termination

A possible extension of the deformation zone ZSMNE012A is examined within an alternative geometry denoted as model GEO2. This implies that ZSMNE012A terminates against the deformation zones ZSMNE018A and ZSMNE004A, instead of against ZSMNE004A. Figure 3-24 shows the vertical sections through the GEO2 model. The broken circle, marked on section AA' indicates the difference compared to the model GEO1 (compare with Figure 3-3). In the GEO2 case more rock blocks are free to move compared to the GEO1 case.

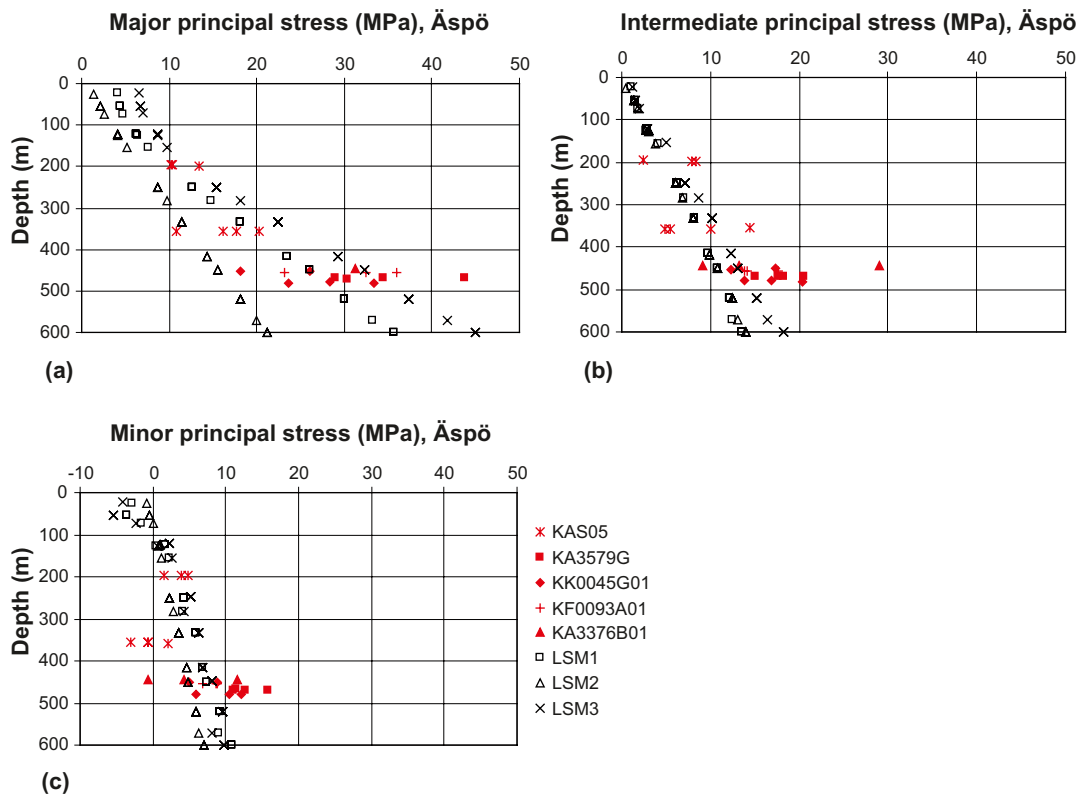


Figure 3-22. Comparison between measured and modelled stresses at Äspö; (a) Major principal stress, (b) Intermediate principal stress, (c) Minor principal stress.

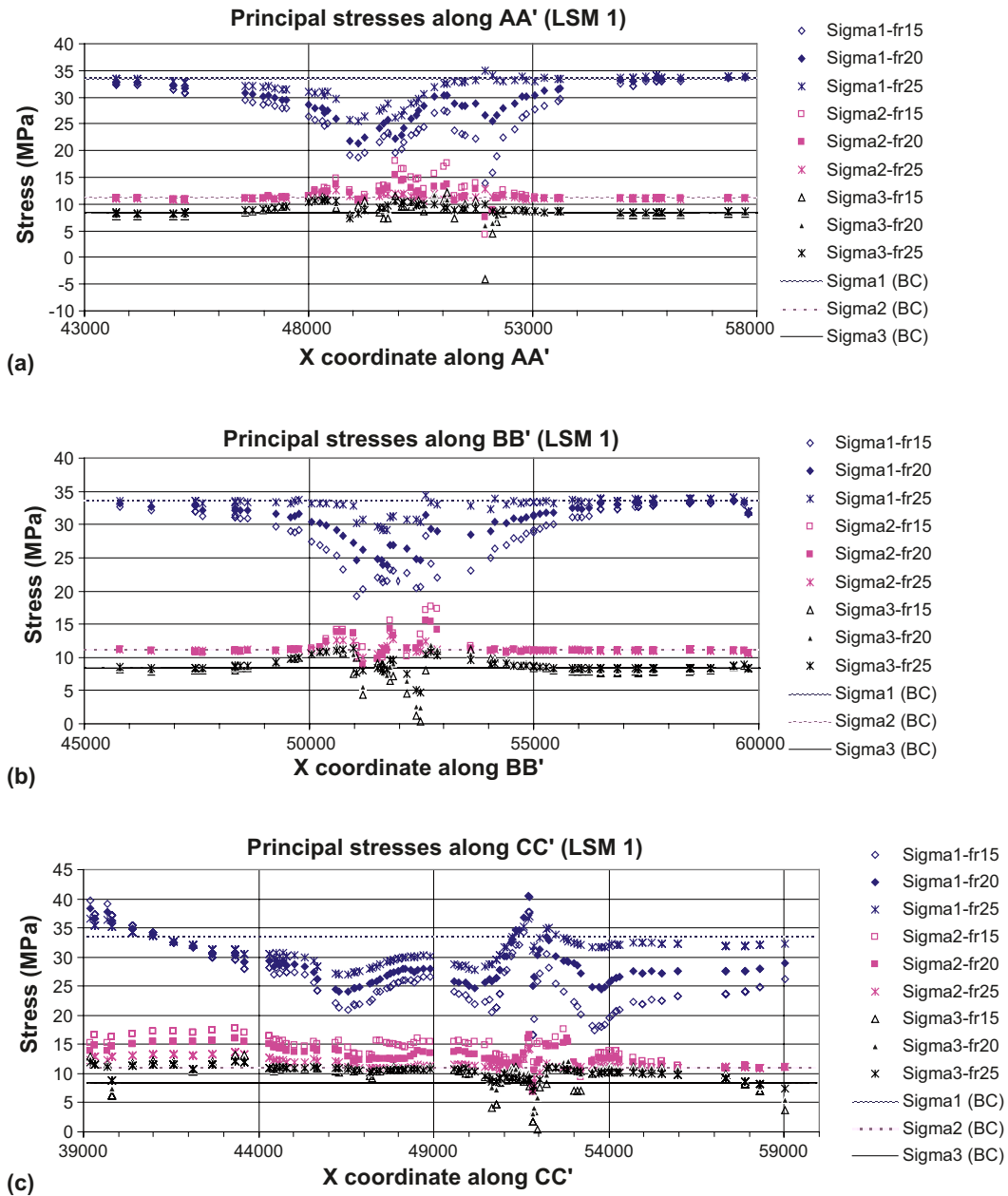


Figure 3-23. Stress distribution along sections AA', BB' and CC' with different friction angles applied to the deformation zones; (a) section AA', (b) section BB', (c) section CC'.

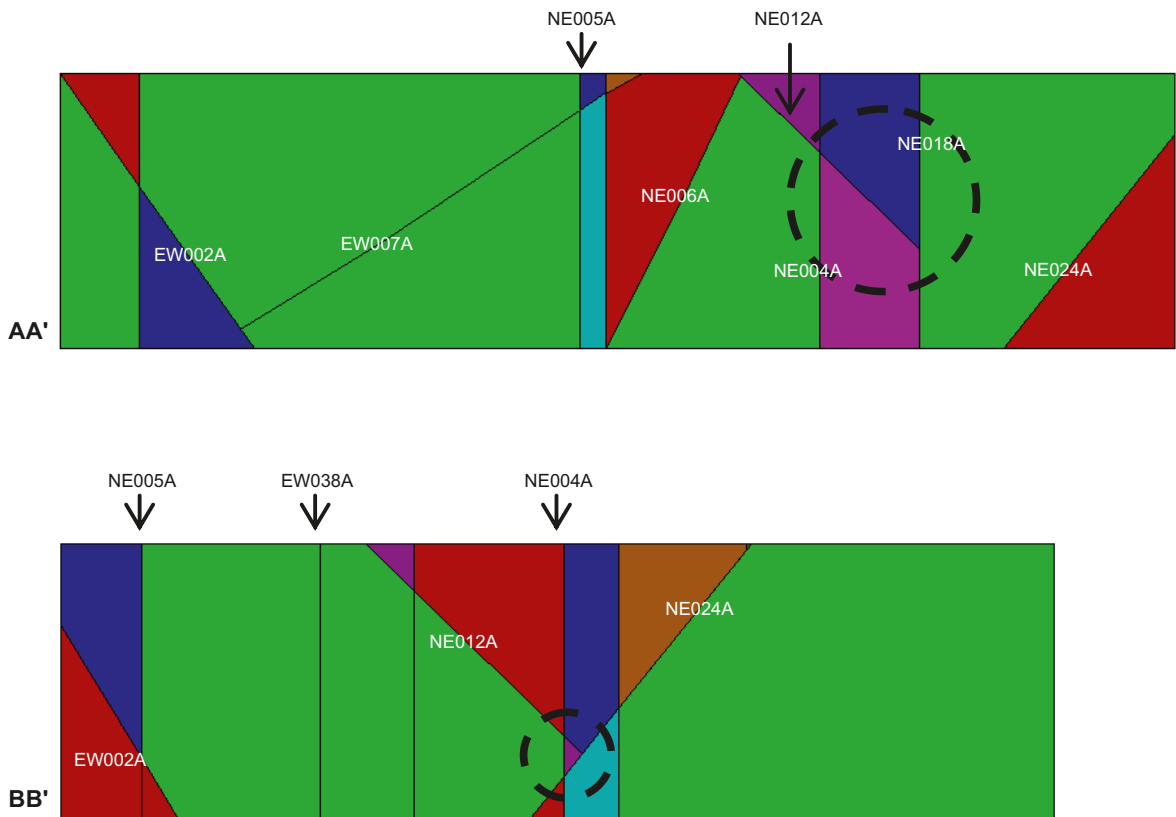


Figure 3-24. Vertical sections through the local model from the entire model GEO2; Broken circles are marked on the sections to indicate differences with the model GEO1 (cp. Figure 3-3).

Figure 3-25 presents the principal stresses along a horizontal line at 450m depth in the vertical section CC', for the GEO2 case. The stress variation along the scan line is smoother compared to the result for case GEO1 (Figure 3-10). These results illustrate the influence termination might have, in particular locally, on the state of stress. In the numerical models the differences are sharp since the geometries are sharp, which they may not be in nature. However, also in reality the stress levels should be expected to change locally depending on the details of zone properties such as terminations.

Figure 3-26 shows a comparison of modelled stresses along sections AA' and BB' computed for models GEO1 and GEO2. Greater stress relaxation is observed in GEO2 where larger shear displacements can occur as shown in Figure 3-27. Figure 3-28 presents comparison between measured and modelled principal stresses at borehole KAV04A. The measurements seem to be closest to results in model LSM2, which is different from comparison results in other boreholes. However, unfortunately the comparison can not be used to distinguish between the two geometrical cases GEO1 and GEO2,

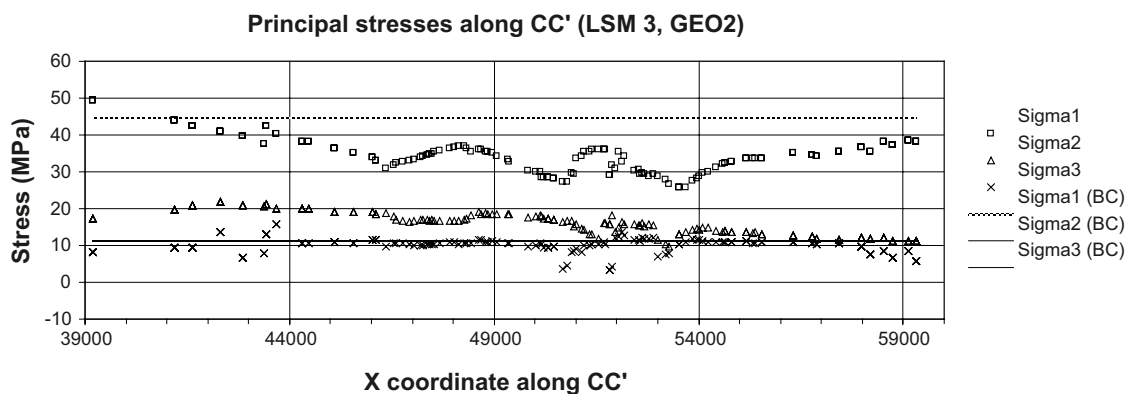


Figure 3-25. Principal stresses along reference the W-E striking section CC', at 450 m depth, with GEO2 model (LSM3). (This diagram may be compared to the diagram from GEO1 model in Figure 3-11 c).

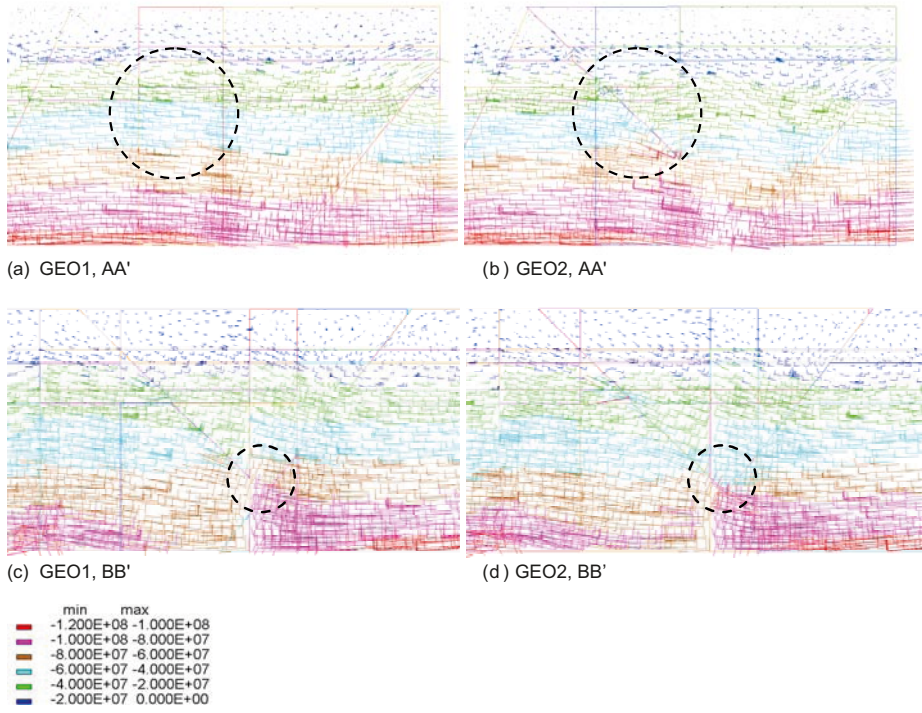


Figure 3-26. Comparison of the in situ stresses computed for models GEO1 and GEO2, respectively, along vertical sections AA' and BB' (located near KAV04A).

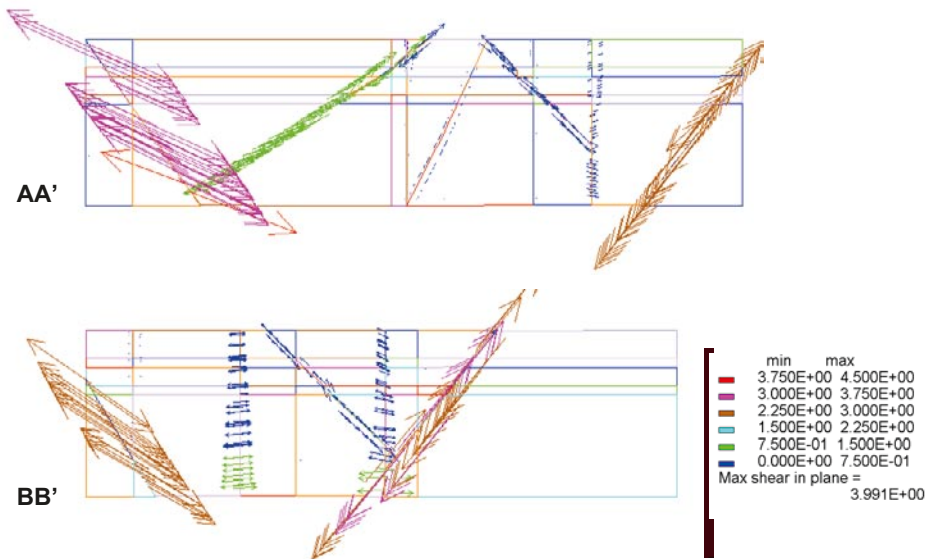


Figure 3-27. Shear displacement in deformation zone within the local model for model case GEO2. This may be compared to results from case GEO1 in Figure 3-9.

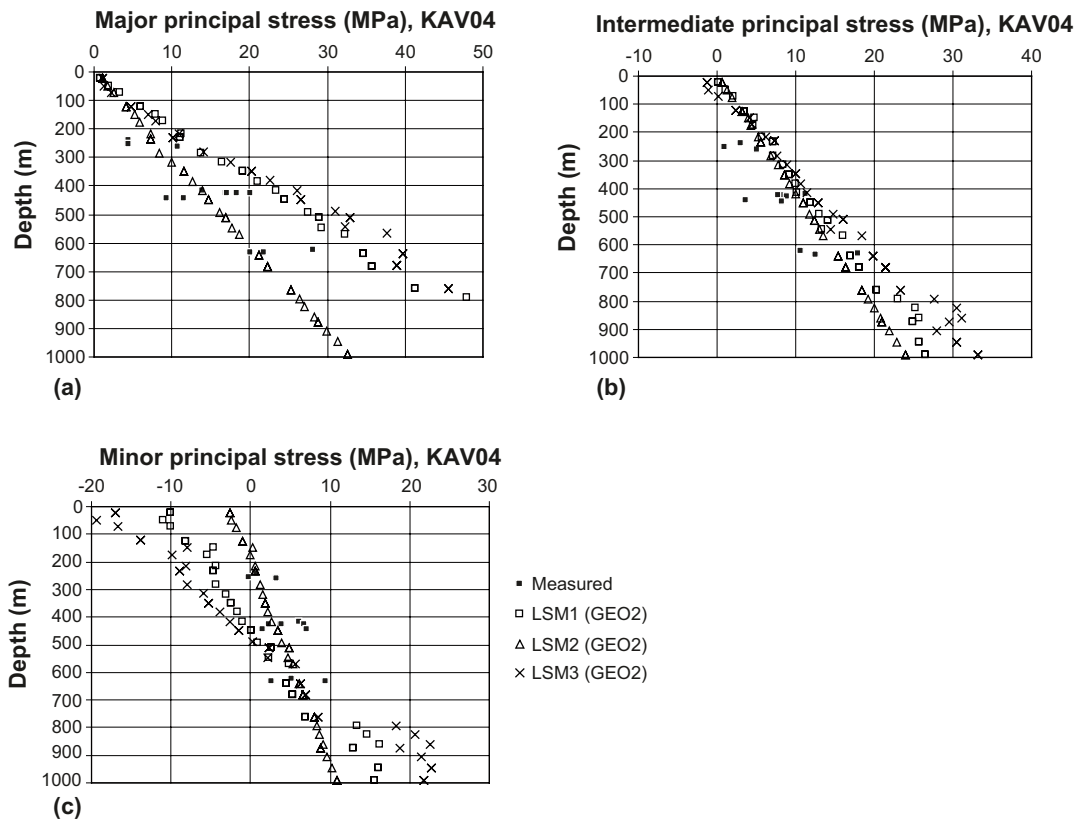


Figure 3-28. Comparison between measured and modelled principal stresses at KAV04A for the GEO2, (a) Major principal stress, (b) Intermediate principal stress, (c) Minor principal stress.

or to confirm the stress increase at depth seen in LSM1 and LSM3, since all the measurements are located above the borehole intersection with the deformation zone. Looking at the map of Simpevarv (Figure 2-1 and Figure 3-1) it may also be concluded that borehole KAV04A is close to a deformation zone (ZSMNE004A), and also fairly sub-parallel to this zone, and therefore the actual geometry of structural features that may influence the stresses at the hole might be more complicated than what is captured in the numerical model.

3.9 Conclusions from numerical modelling

Numerical analyses were conducted to model the state of stress in Laxemar model volume using a three-dimensional distinct element code, 3DEC /Itasca 2003/. Different cases of far field stress were applied on the geometrical model that represented the deformation zones as planar discontinuities. Measured and modelled stresses are compared in order to choose the numerical model that best fits the measured data. Numerical analyses were also used for the prediction of stress variation which is useful information for the planning of future measurement campaigns. Despite some discrepancies between the measured and the modelled stress, numerical modelling seems to be an effective tool to improve the understanding of the state of stress in situ. The main conclusions from the numerical modelling are summarized as follows:

1. The modelled state of stress is closely related to the geometry of large-scale deformation zones identified in the region. Significant decrease in maximum principal stress and change in their orientation were observed due to slip failure on deformation zones.
2. The change of stress is more significant when the deformation zones are more optimally oriented for sliding under the given in situ stress conditions. The change in stress magnitude depends on the condition for the sliding of fractures. The initial boundary condition of stress and the selection of frictional properties are most important factors that determine the state of stress with the given geometry of fractures.

3. The modelled stress at KLX04 matched the measured stress well and a sudden increase of stress in the borehole is explained by the influence of the deformation zone ZSMEW007A.
4. The modelled stress at KAV04A slightly overestimated the measured stress and this needs further investigation. The modelled stress at Äspö area matched the measured stress moderately.
5. Stresses at KLX09 and KLX10 were predicted using numerical modelling (not presented in this report). The influence of deformation zone ZSMEW007A is anticipated and stresses at KLX09 are expected to be lower than those at KLX10. (No measurements are planned to be performed in these boreholes).
6. The trend of the major horizontal stress varies only slightly over the model volume, also when the deformation zones are at slip failure.

Among the three different stress model cases, the case LSM3 shows in general the results closest to the measurements results, and therefore this model was selected as a base, together with the measurement results, for the descriptive model for the state of stress at Laxemar model area. This will be described in the following chapter.

4 Model for the state of stress at Laxemar

4.1 Stress domains

The stress modelling is mainly based on the stress measurement data presented in Section 2. As the measurement data show a large spread, a geological explanation had to be sought. Following the developed methodology, the most probable explanation for the noted variation was expected to be associated with the existing structures (i.e. the modelled deformation zones). The deformation zone model, presented in Section 3.2, includes both the interpreted geometry and a description of the properties of the interpreted major zones.

It was recognised that the deformation zones essentially trending northeast on either side of the Simpevarp peninsula – Hålö – Ävrö (zones ZSMNE012A and ZSMNE024A) formed a wedge-shaped body of rock that could show a different stress regime compared to areas further to the west. If the measured stress data is sorted into two different groups, representing these assumed geographical domains (cf. Figure 4-1 and Figure 4-2), it is noted that the spread within each group is significantly less than the overall spread of the two groups merged together. This fact provides some support for the hypothesis made and it was assumed that the measurement data, no matter including some uncertainty, could be associated with the two suggested stress domains.

A second possible stress model would be that the stresses locally vary much and that the variation is unrelated to the existing deformation zones. This model is the simplest one and was earlier adopted for the Simpevarp version 1.1 at the time when data were very limited. A third model could be that there

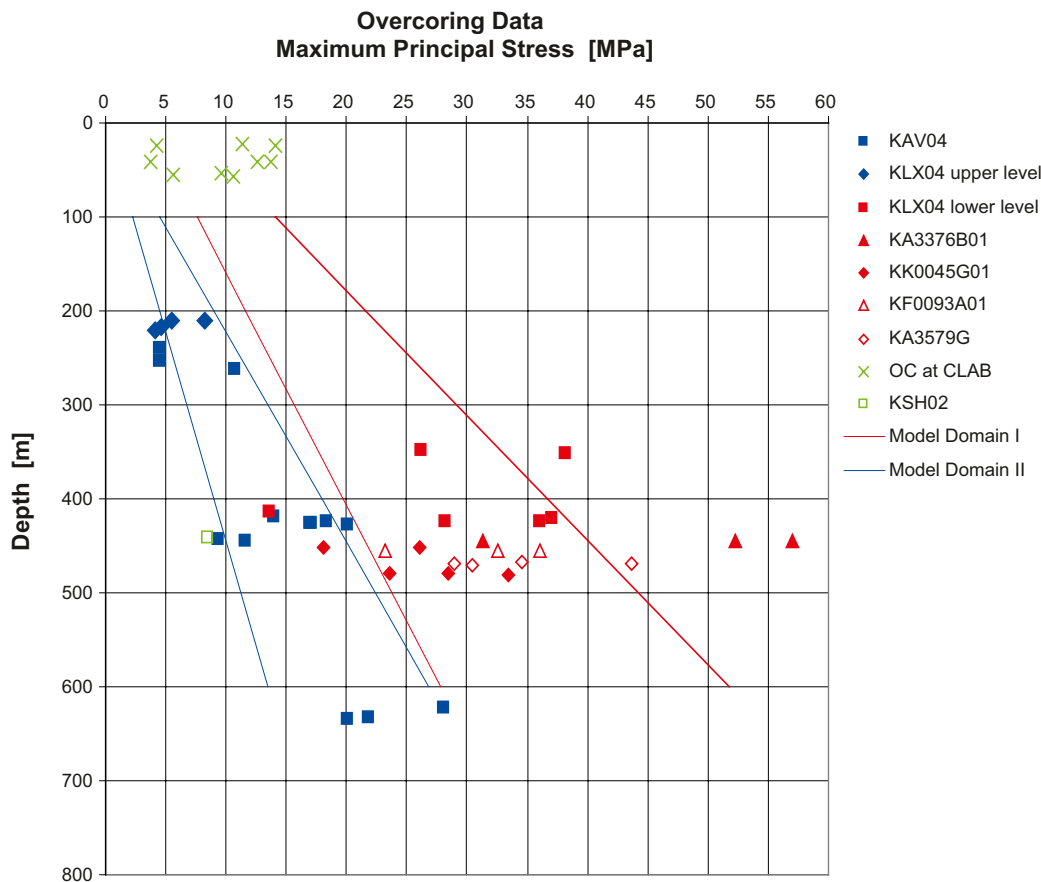


Figure 4-1. Maximum principal stress from measurements, sorted depending on location in the different stress domains, I (red) and II (blue). Note the KLX04 data are therefore divided. The data from CLAB and KSH02 (green) are uncertain in terms of reliability. The uncertainty span for the stress models is shown as solid lines.

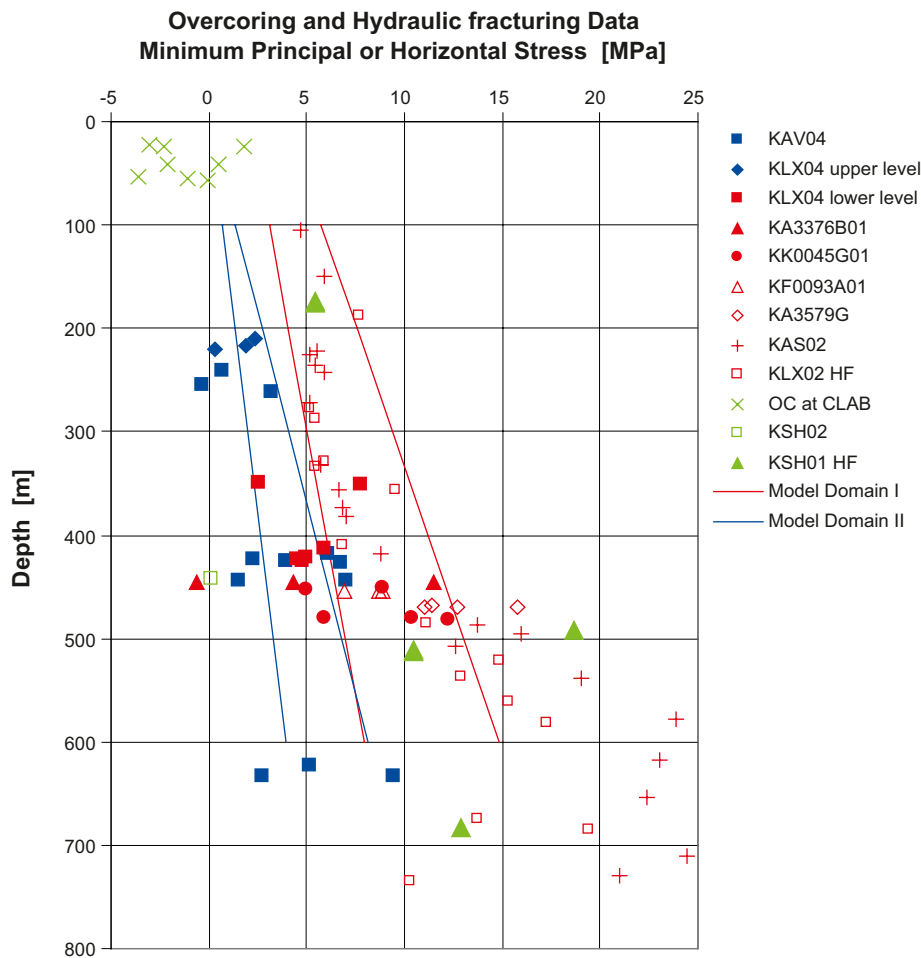


Figure 4-2. Minimum principal stress magnitude from measurements, sorted depending on location in stress domain, I (red) or II (blue). Data from CLAB and KSH02 are uncertain in terms of reliability, and data from borehole KSH01A, passing through several deformation zones are also uncertain in terms of domain.

indeed exist structurally controlled stress domains, but that the positions and geometry of these important structures are different from those reported. If the geologically modelled deterministic deformation zones change in a later phase of the site-descriptive model, this alternative model should be considered.

In Table 4-1 through Table 4-4, the stress estimations are presented for the two defined stress domains included in the local model area. The locations of the two stress domains are shown in Figure 4-3. In this figure, the defined stress domains and their relation to the major deformation zones are shown, for this model version Laxemar 1.2.

Note that division into two stress domains is based on available information up to the time of writing this report. This model may be changed at later stages of the site investigation and modelling efforts when new measurement data become available.

The mean principal stress magnitudes are estimated, giving a most likely value and a possible span and the magnitudes are furthermore assumed to increase with depth. The model describes the state of stress between 100 and 1,100 m depth. The mean stress values, as given, are the expected mean stress values in a cubical rock volume of 30×30×30 m size. The uncertainty is described as a percentage of the mean value.

Table 4-3. Predicted in situ stress orientations in the Simpevarp 1.2 stress domain I.

Parameter	σ_1 trend/plunge	σ_2 trend/plunge	σ_3 trend/plunge
Mean stress orientation	132/0	90/90	42/0
Uncertainty	$\pm 15/\pm 10$	$\pm 90^2/\pm 15-45^1$	$\pm 15/\pm 15-45^1$
Spatial variation, rock domains	$\pm 15/\pm 15$	$\pm 15/\pm 15$	$\pm 15/\pm 15$
Spatial variation inside or close to deformation zones	$\pm 25/\pm 30$	$\pm 25/\pm 30$	$\pm 25/\pm 30$

1) At some level σ_2 and σ_3 may have similar magnitude and the plunge can then be any. The three principal stresses are in each point oriented perpendicular to each other.

2) Since the direction is expected to be sub-vertical, i.e. the plunge 90, the trend of the tensor may be any.

Table 4-4. Predicted in situ stress orientations in the Simpevarp 1.2 stress domain II.

Parameter	σ_1 trend/plunge (deg/deg)	σ_2 trend/plunge (deg/deg)	σ_3 trend/plunge (deg/deg)
Mean stress orientation	132/0	90/90	42/0
Uncertainty	$\pm 20/\pm 20$	$\pm 90^2/\pm 15-45^1$	$\pm 20/\pm 15-45^1$
Spatial variation, rock domains	$\pm 15/\pm 15$	$\pm 15/\pm 15$	$\pm 15/\pm 15$
Spatial variation inside or close to deformation zones	$\pm 25/\pm 30$	$\pm 25/\pm 30$	$\pm 25/\pm 30$

1) At some level σ_2 and σ_3 may have similar magnitude and the plunge can then be any. The three principal stresses are in each point oriented perpendicular to each other.

2) Since the direction is expected to be sub-vertical, i.e. the plunge 90, the trend of the tensor may be any.

4.3 Model for principal stress orientations

The model for the stress orientation was selected based on the measurement data in the different boreholes. To avoid much bias towards results at Äspö with many data points and to reflect the results from as large spatial coverage as possible the median orientation for each borehole was first calculated. The results from borehole KAS03, KAS05, KSH02 and KOV01 (OC) were excluded since the data quality was judged poorer. The data from CLAB was excluded since the more shallow measurements are expected to show larger spread for orientation, and are thus less reliable. Further these data are older and of lower quality. The mean of the trend value from the remaining ten boreholes became 132 degrees from north. Both results from hydraulic fracturing and overcoring were included in the estimation.

The uncertainty span was judged (not calculated) such that the span would cover a large part of the measurement data, and all borehole average values. The numerical model has indicated that even when the major deformation zones do influence the stress magnitudes and give slip on the fractures the overall orientation of the stress direction will remain the same over the whole area. Therefore the same orientation was assumed for both stress domains and no sorting of data was made in the estimation.

4.4 Uncertainty and variation in the stress model

There are several sources of uncertainty in the stress model. Firstly, the accuracy of the borehole measurements is limited. The accuracy of the results made by overcoring method is dependent on accuracy in laboratory biaxial tests for the interpretation of magnitudes. The hydrofracturing method is dependent on ambiguities in interpretation of the pressure build-up curves. Secondly, the normally available data is not large, from a statistical viewpoint. The fitted linear stress profile has an uncertainty due to this. Thirdly, the assumptions made regarding the stress domains and the need to extrapolate the available measurement results over large areas also incorporate a degree of uncertainty. The value selected for the total uncertainty, as a result, includes different components and is selected based on a judgement made for each. The selected spans are shown graphically in Figure 4-1 and Figure 4-2 and it can be seen that most of the observed data are enclosed in the model uncertainty span selected, i.e. the span between the red and the blue lines, respectively.

Spatial variation is, in contrast to the uncertainty, the expected actual local (horizontal) variation in the stresses measured, which may be taken as a value roughly representing one cubic meter. Following the strategy report for stress modelling /Hakami et al. 2002/ the spatial variation is described with a new percentage span around the mean value. Inside the rock mass (including natural fractures), but outside the major deformation zones, the spatial variation of the stress is expected to be less than variation taking place within the immediate vicinity of the deformation zones.

References

SKB's (Svensk Kärnbränslehantering AB) publications can be found at www.skb.se/publications.

Bjarnason B, Klasson H, Leijon, B, Strindell L, Öhman T, 1989. Rock stress measurements in boreholes KAS02, KAS03 and KAS05 on Äspö. SKB PR-25-89-17, Svensk Kärnbränslehantering AB.

Chryssanthakis P, Tunbridge L, 2003. Borehole: KSH01A Determination of P-wave velocity, transverse borehole core. Oskarshamn site investigation. SKB P-03-106, Svensk Kärnbränslehantering AB.

Chryssanthakis P, Tunbridge L, 2004a. Borehole: KSH02A Determination of P-wave velocity, transverse borehole core. Oskarshamn site investigation. SKB P-04-11, Svensk Kärnbränslehantering AB.

Chryssanthakis P, Tunbridge L, 2004b. Borehole: KAV01 Determination of P-wave velocity, transverse borehole core. Oskarshamn site investigation. SKB P-04-43, Svensk Kärnbränslehantering AB.

Chryssanthakis P, Tunbridge L, 2004c. Borehole: KLX02 Determination of P-wave velocity, transverse borehole core. Oskarshamn site investigation. SKB P-04-45, Svensk Kärnbränslehantering AB.

Hakami E, Hakami H, Cosgrove J, 2002. Strategy for a rock mechanics descriptive model. Development and testing of an approach to modeling the state of stress. SKB R-02-03. Svensk Kärnbränslehantering AB.

Hakami E, Min K-B, 2005. Modeling of the state of stress. Preliminary site description of Simpevarp subarea – version 1.2. SKB R-05-19. Svensk Kärnbränslehantering AB.

Itasca Consulting Group Inc, 2003. Three-Dimensional Distinct Element Code – User's Guide, Minneapolis, Minnesota, USA.

Janson T, Stigsson M, 2002. Test with different stress measurement methods in two orthogonal boreholes in Äspö HRL. SKB R-02-26, Svensk Kärnbränslehantering AB.

Klasson H, Persson M, Ljunggren C, 2001. Äspö Hard Rock Laboratory. Overcoring rock stress measurements at the Äspö HRL. Prototype Repository: Borehole KA3579G (Revised data) and K – tunnel: Borehole KK0045G01. SKB IPR-01-67, Svensk Kärnbränslehantering AB.

Klasson H, Lindblad K, Lindfors U, Andersson S, 2002. Äspö Hard Rock Laboratory. Overcoring stress measurements in borehole KOV01, Oskarshamn. SKB IPR-02-18, Svensk Kärnbränslehantering AB.

Klee G, Rummel F, 2002. Äspö Hard Rock Laboratory. Rock Stress measurements at the Äspö HRL. Hydraulic fracturing in boreholes KA2599G01 and KF0093A01 SKB IPR-02-02, Svensk Kärnbränslehantering AB.

Lindfors U, 2004. Oskarshamn site investigation. Hydraulic fracturing and HTPF rock stress measurements in borehole KSH01A. SKB P-04-310, Svensk Kärnbränslehantering AB.

Ljunggren C, H Klasson, 1997. Drilling KLX02 – Phase 2 Lilla Laxemar Oskarshamn – Deep hydraulic fracturing Rock stress measurements in Borehole KLX02, Laxemar. SKB PR U-97-27, Svensk Kärnbränslehantering AB.

Rummel F, Klee G, Weber U, 2002. Äspö Hard Rock Laboratory. Rock Stress measurements in Oskarshamn. Hydraulic fracturing and core testing in borehole KOV01. SKB IPR-02-01, Svensk Kärnbränslehantering AB.

Sjöberg J, 2003. Äspö Hard Rock Laboratory. Äspö Pillar Stability Experiment. 3D overcoring rock stress measurements in borehole KA3376B01 at Äspö HRL. SKB IPR-03-16, Svensk Kärnbränslehantering AB.

Sjöberg J, 2004a. Oskarshamn site investigation. Overcoring rock stress measurements in borehole KAV04. SKB P-04-84, Svensk Kärnbränslehantering AB.

Sjöberg J, 2004b. Overcoring rock stress measurements in borehole KSH02. SKB P-04-23, Svensk Kärnbränslehantering AB.

Sjöberg J, Perman F, 2005. Oskarshamn site investigation. Overcoring rock stress measurements in borehole KLX04. SKB P-05-69, Svensk Kärnbränslehantering AB.

SKB, 2004. Preliminary site description, Simpevarp area – version 1.1. SKB R-04-25, Svensk Kärnbränslehantering AB.

SKB, 2006. Preliminary site description, Laxemar subarea – version 1.2. SKB R-06-10, Svensk Kärnbränslehantering AB.